UNIVERSITÀ DI PISA

Dipartimento di Farmacia

Corso di Laurea Specialistica in Chimica e Tecnologia Farmaceutiche

Tesi di Laurea:

Rational design, synthesis and evaluation of heterocyclic derivatives as inhibitors of serine palmitoyltransferase

Relatore:

Dott.ssa Sara Del Carlo

Dott. Giuseppe Saccomanni

Correlatore:

Prof.ssa Clementina Manera

Candidato:

Reinhold Baci **(N° MATRICOLA 408866)**

Settore Scientifico Disciplinare: **CHIM-08**

ANNO ACCADEMICO 2012 – 2013

SECRETAZIONE DELL' ELABORATO SCRITTO DELLA TESI DI LAUREA

"Il contenuto di questa tesi di laurea è strettamente riservato, essendo presenti argomenti tutelati dalla legge come segreti. Pertanto tutti coloro che ne prendono conoscenza sono soggetti all'obbligo, sanzionato anche penalmente dagli articoli 325 e 623 del codice penale, di non divulgare e di non utilizzare le informazioni acquisite."

INDEX

INTRODUCTION

1.1 Introduction

More than 100 hundred years ago, Johann L. W. Thudicum described a not well identified aliphatic alkaloid in the brain called sphingosine[1]. The structure of this substance was characterized only 50 years later by Carter at al.[2]

In the last years, structural and distribution studies have highlighted the critical roles of sphingolipids in membranes micro domains formation, skin barrier function and modulate on of cellular events like apoptosis, proliferation and differentiation[3-5].

These discoveries along with bioactive signal function observation, increase research attraction and attention on sphingolipids metabolism[6-11].

1.2. Sphingolipids

Sphingolipids (SPL) are one of eight categories of the LIPID MAPS classification system and they are described as lipids containing a sphingoid base (1,3-dihydroxy-2-amino alkane) linked by an amido group to a fatty acid and with polar headgroup, like phosphate and carbohydrate[12]. SPL distribution appears ubiquitous in eukaryotic. In particular, SPL alkane group is usually an eighteen carbons chain; C-2 and C-3, in the polar headgroup, are chiral and the configuration is 2S, 3R, D-Eritro. Indeed, in mammal cells, sphingosine appear to be the major sphingoid base, followed by dihydrosphingosine, while phytosphingosine, the third major type of sphingoid bases, has been found mainly in plants, although it was revealed in large amount in mammal tissues like stomach and kidney. Sphingolipids containing cholinephosphoceramide, known as sphingomielyn, represent 5-10% of mammalian membrane's phospholipids. SPL are produced also by some prokaryotes, plants, bacteria and fungi through different biosynthetic pathways [1,12]. In fungal and plants inositol-phosphoceramide is the most abundant constituent of the membrane phospholipids; these observations suggest a relevant structural dissimilarity in the polar headgroup in different species. Conversely the polar headgroup of glycerophospholipids are structurally very similar between mammal cells and fungi[12] (Fig.1).

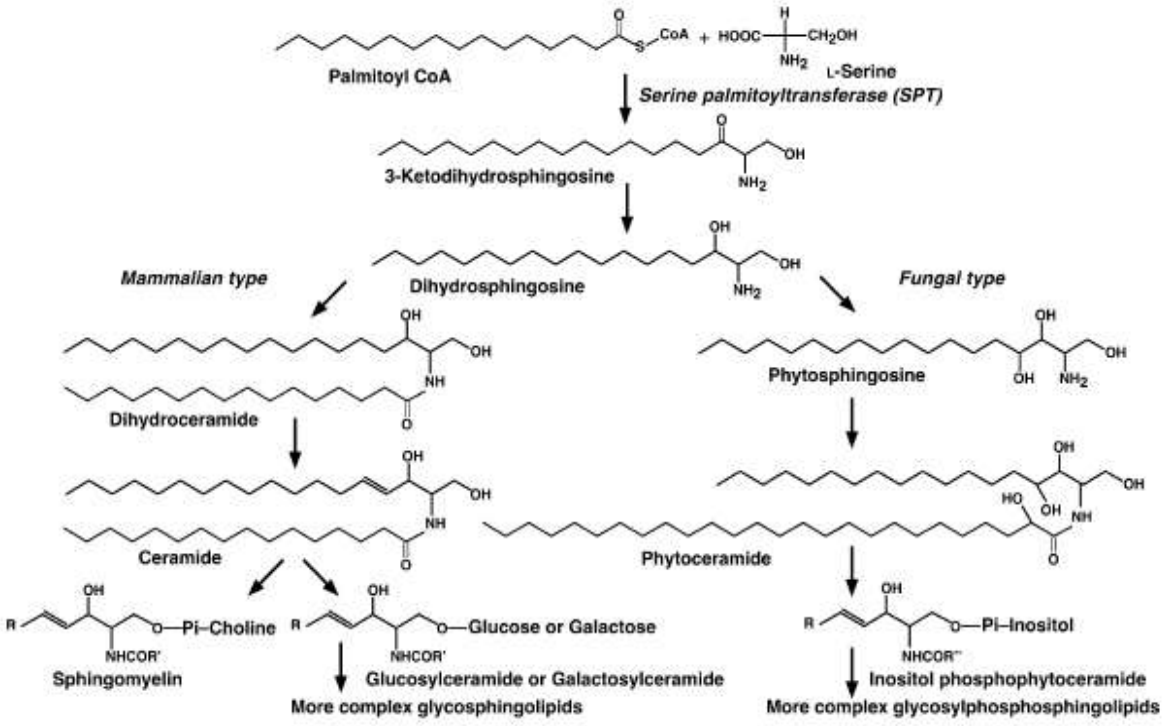

Fig. 1: *Biosynthetic pathway of sphingolipids in mammalian and fungal cells.*

1.2. Ceramide

Several studies performed by Braun[13], and Stoffel [14], independently, have demonstrated in 1968 that the second step of sphingolipid biosynthesis is the NADPH-dependent reduction of a C-3 carbonyl group leading to dihydrosphingosine[15]**.** In mammalian cells, dihydrosphingosine undergoes to an N-acylation reaction forming dihydroceramide. Afterwards, an alkyl chain oxidation leads to ceramide which successively functionalized at the polar headgroup to give sphingomielyn or different glycosphingolipids. Conversely, in fungi, dihydrosphingosine undergoes to oxidation and then to N-acylation forming phytoceramide which is further converted in inositol phosphophytoceramide and more structurally complex derivates. In fungi, the acyl-chain is mainly represented by C-26 hydroxy fatty acid, whereas mammal ceramide deerivatives are saturated C-16/C-24 fatty acid chain[16,17]. Cells produce sphingolipids through two different metabolic ways: catabolic and anabolic pathways. The catabolic pathway involves hydrolyses of complex molecules, as sphingomielyn and glucosphingolipid, to obtain ceramides. The anabolic pathway (also called *de novo* biosynthesis) provides an enzymatic cascade which leads to the formation of ceramides starting from simple and abundant substrates like L-serine and palmitoyl-CoA[1].

2. Serine palmitoyltransefarse (SPT)

Sphingolipids biosynthesis is different between species (i.e. *S. cerevisiae* produces phosphoinositol headgroup sphingolipids only, while *P. pastoris* both glucosylceramide and phosphoinositol sphingolipids headgroup), whereas the first enzymatic step of *de novo* biosynthesis is conserved across all species producing sphingolipids[2] (Fig.2). The common step of the *de novo* synthesis is an enzymatic condensation carried out by serine palmitoyltransferase (SPT), a pyridoxal-5'-phosphate (PLP) dependent enzyme. SPT is an enzyme belonging to alfa-oxoamine synthase (AOS) family which is a PLP dependent family.

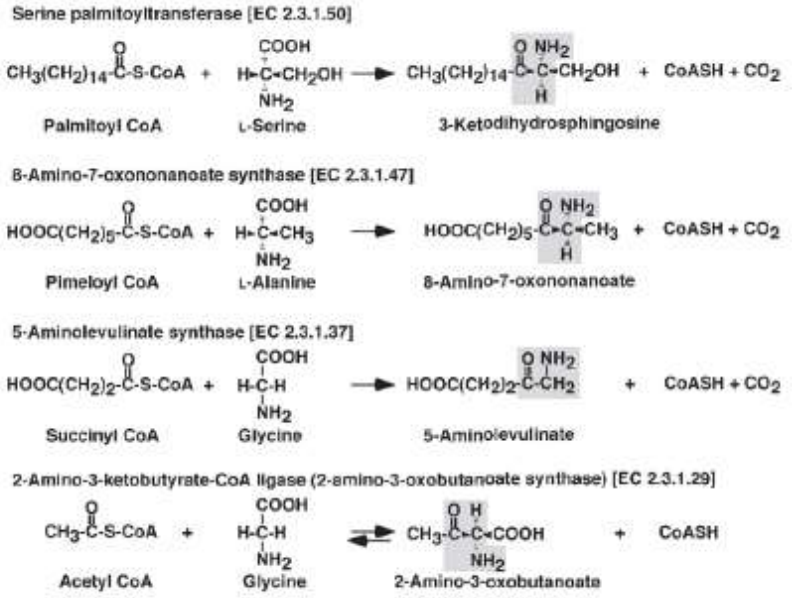

Fig. 2: *POAS family. Reactions catalyzed by POAS family members.*

SPT catalyzes a condensation between L-serine and typically C16 acyl-CoA thioester (palmitoyl-CoA), to give a Claisen-like C18 condensation product: 3-ketodihydrosphingosine (KDS). Successively KDS is rapidly reduced to dihydrosphingosine in presence of NADPH[1,2]. SPT plays a key role in the biosynthesis of sphingolipids indeed regulation of SPT catalyzed step prevents accumulation of sphingolipids metabolites (i.e. sphingoid base) while inhibition of later biosynthetic steps lead to metabolite accumulation which are death effectors in various experimental models and pathological conditions. Therefore, SPT condensation reactions represent the rate-limiting step of sphingolipids biosynthesis[1].

2.1. Bacterial SPT

The first three dimensional structure of SPT was obtained by the isolation of the homodimeric (and water soluble) SPT from the Gram-negative bacterium *S. paucimobilis* (spSPT)[18]. The crystal structure reveals that the holo-SPT monomer (or internal aldimine) consists of three domains: the N-terminal, the central catalytic domain and the C-terminal domain. The N-terminal domain is consist of 80 residues (an α-helix followed by 3 β-sheets). This domain is linked with the central domain also called catalytic domain. In the central domain is recognized the Lys^{265} residue responsible of PLP cofactor binding, while 7 β-sheet is composed by about 200 residues. The C-terminal domain is strictly linked with N-terminal domain by binding interactions[19]. Three dimensional crystal of the holo-enzyme revealed a homodimeric structure containing a conserved Lys^{265}-binding-PLP residue. However, for the correct positioning of the PLP cofactor, (crucial for the catalytic activity), π-stacking interactions between the pyridine ring and His^{159} are required. PLP interacts also with other residues such as Asn^{138}, Asp^{231}, His^{234}, Thr^{262}, Gly^{134} and Tyr^{135}. Furthermore, an Arg^{379} is needed for the positioning of the L-serine in the catalytic site because of crucial interaction with the carboxy moiety of the substrate[**1**].

Other SPT homologues, like *Sphingobacterium multivorum* SPT (SmSPT) and *Sphingobacterium wittichii* (SwSPT), exhibit difference at few levels. SmSPT have a 70% sequence identity and in active site the external aldimine (formed by the PLP and serine) is linked by two water molecules to two aminoacid residues, Ser^{81} and Met^{271}, and (not to a Lys)[20]. Three-dimensional structure of SwSPT reveals a larger active site than in SpSPT, probably because of the use of a larger acylated-ACP thioester substrate[21,22].

2.2. Eukaryotic SPT

Eukaryotic SPT is a heterodimer consisting in two subunits, LCB1 and LCB2, both linked to endoplasmatic reticulum (ER) and they are encoded by two different genes, lcb1 (SPTLC1) and lcb2 (SPTLC2), composed by 15 exons of 85 kbp size localized on chromosome 9, arm q21-q22, and 12 exons of 110 kbp size localized on chromosome 14, arm q24.3-q3 respectively. These genes encode for proteins of 53 and 63 kDa, with 20 % sequence identity that is probably critical for dimerization[23,24]. LCB proteins have 95% identity between mammals and 40% between mammals and yeast. The sequencing of SPTLC1 and SPTLC2 genes in *Saccharamyces cerevisiae* revealed that the active site of eukaryotic SPT is localized in the LCB2 subunit; this observation is suggested by detection of conserved residues of AOS's family (one lysine, two hystidine and an aspartate) which are essential to lock the PLP cofactor in the active site[1,2]. LCB1 subunit appears crucial for SPT's catalytic activity. The lack of this subunit expression or a missense mutation in SPTLC1 gene causes alteration of SPT's catalytic activity[25]. Furthermore, CHO cells line defective in SPTLC1 transcription express lower levels of LCB2. To obtain an overexpression of LCB2 is required an overexpression of LCB1 and LCB2. Moreover, it appears to be unstable when it is not associated with the LCB1. On contrary an high level of LCB1 do not require an overexpression of LCB2. Both monomers have only one highly hydrophobic transmembrane domain (TMD). The catalytic site has a cytosolic orientation indeed indirect immunocytochemical analysis indicated that C-termini and N-termini of LCB1 have cytosol and lumen orientation respectively[26]. LCB1 and LCB2 are ER membrane integrated proteins type I. Another isoform of LCB2 called LCB3 is expressed only in certain tissues.

In yeast this enzyme is constituted by the so called "SPOTS COMPLEX" that's encodes for SPT–ORM1/2-Tsc3-Sac1 (phosphatase)[27]. Therefore, LCB1 and LCB2 subunits are associated with a third subunit, Tsc3, which is required for the maximal SPT activity. This heterodimeric structure is associated with oromucosoids proteins (ORM1/2) which are able to negatively regulate SPT.

Recently for human SPT two novel small subunits named ssSPTa and ssSPTb were discovered. These subunits can enhance activity >10 fold when bound to LCB1-LCB2 heterodimer. Moreover orosomucoid-like (ORMDL) proteins appear to be able to interact with the LCB1-LCB2 heterodimer[28].

2.3. Substrate

Palmitoyl-CoA is the more kindred acyl-CoA thioester substrate of SPT in mammalian cells; on the other hand pentadecanoyl-CoA and heptadecanoyl-CoA are also good substrates less abundant. L- and D- serine are SPT amino acid substrates. SPT is able to form the Schiff's bases with both enantiomers but the alfa-deprotonation step (before acylation) proceeds only with L-serine substrate. Thus L-serine is the common SPT's substrate in the *de novo* synthesis. The hydroxyl, carboxyl and amino groups of L-serine appear to be necessary for interaction with SPT; neither L-alanine, L-serinamide, D,L-serinol and nor L-serine methyl ester not in the formation of [^{3}H]KDS from L-[^{3}H]serine, indicating that the hydroxyl, amino, and carboxyl groups of L-serine are responsible for the recognition of the amino acid substrate by the SPT enzyme[29].

3. Reaction mechanism

SPT catalyzes a Claisen like condensation of L-serine and palmitoyl-CoA which leads to 3-KDS as final product. SPT reaction mechanism proceeds across six step: 1) formation of the Schiff base between L-serine and PLP, 2) L-serine α-hydrogen removing; 3) nucleophilic attack to palmitoyl-CoA (formation a transient acylated adduct), 4) decarboxylation, 5) protonation of α-carbanion and 6) KDS release (Fig.3). Assays conducted with purified enzyme from chinese hamster ovary cell, suggested that one molecule of mammalian SPT is capable of catalyzing maximally of 80 cycles of these steps per minute[30].

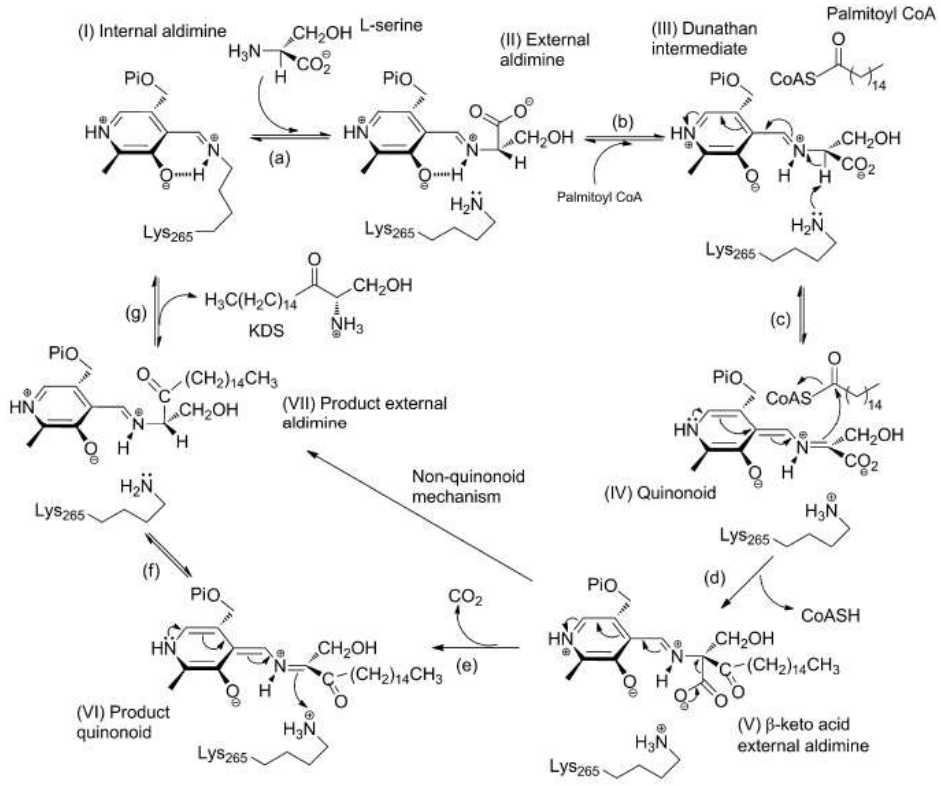

Fig. 3: *Catalytic mechanism of SPT.*

The PLP cofactor catalyses all the reaction mechanism. Interaction of PLP aldehyde group and Lys[265] lead to a Schiff base (internal aldimine) in the active site. Spectrophotometric analysis of holo SPT revealed two UV absorption peaks which represent two tautomers of the Schiff base PLP-Lys[265]: the enolamine (338 nm) and ketoenamine (426 nm). Moreover, Crystalline structure of *S. Multivorum* and *S. Paucimobilis* SPT highlighted that PLP has Van der Walls interaction with His[159] and Ala[233].

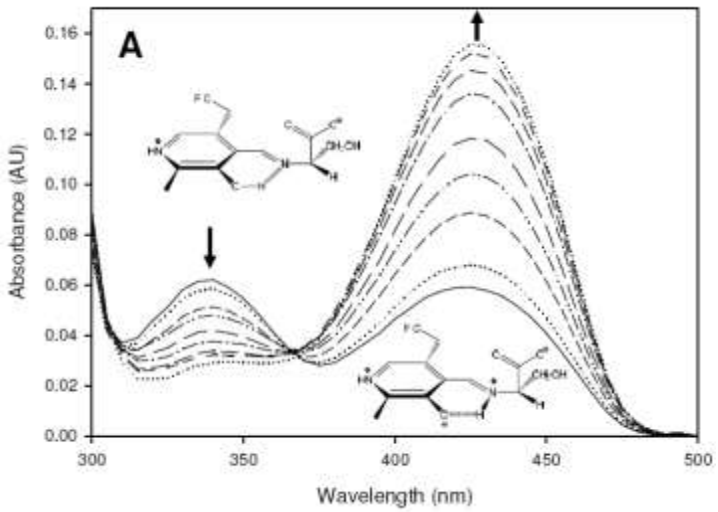

Fig. 4: *Spectrophotometric analysis of holo SPT*

Addiction of L-serine to the holo-enzyme causes drastically changes in the UV spectra due to the formation of a new Schiff base between PLP and L-serine (external aldimine). Two intermediate adducts are identified: first adduct has an absorption similar to holo-SPT while the other one has a maximum peak at 426 nm (which represent the ketoenaminic tautomer of the new Schiff base) (Fig.4). The interaction of PLP with L-serine causes a rotation of pyridine ring or a torsion of the Schiff base C4-C4' bound.

Once the external aldimine is formed, L-serine is conformationally stabilized by interaction of the carboxyl group with His^{159} Nε2 (hydrogen bond) and by interaction of the hydroxylic group with the PLP phosphate group and a molecule of water. These interactions fixed the PLP-L-serine complex allowing a perpendicular orientation (80°) of Cα-COO bond to imine-pyridine plane.

The next step of the reaction mechanism is represented by the formation of a new C-C bond via a Claisen like condensation. Two different intermediate may be involved in the nucleophilic substitution: the decarboxylated intermediate or that one generated after removal of the α-H. In order to understand the intermediate involved in the nucleophilic substitution reaction some experiments have been developed in presence of a palmitoyl-CoA analogue S-(2-oxoheptadecyl)-CoA. This compound has a methylene group inserted between the sulphur atom and the carbonyl groups which doesn't allow the nucleophilic substitution. Data obtained performing the enzymatic reaction in presence

of S-(2-oxoheptadecyl)-CoA and deuterated solvent showed the α-hydrogen switch with the deuterated solvent increase of about 100 times (high peak) at 426 nm. Therefore, α-deprotonation of external aldimine is improved in presence of palmitoyl-CoA substrate and a significative amount of quinoid adduct have been formed. This suggests that the quinoid adduct attack palmitoyl-CoA thioester to form the C-C bond. A faster α-deprotonation of external aldimine in presence of palmitoyl-CoA reduce the risk of intermediates accumulation which can form pyridoxamine-5'-phosphate (PMP) after transamination reaction (PMP can't be converted to PLP thereby the enzyme is inactivated). According to Dunathan hypothesis, the α-deprotonation process takes place when the bond involved in the nucleophilic substitution is perpendicular to the imine-pyridine place. The reaction takes place thanks to the complete overlap between the σ-orbital (occupied) of the designed bond and the free π-orbital of the conjugate imine-pyridine system. The increase of α-deprotonation process in presence of palmitoyl-CoA is related to a strictly stereochemical control of the reaction. In the external aldimine conformation the Cα-H bond is 40° rotated with respect to the imine-pyridine plane avoiding the α-deprotonation process. This conformation is generated by interaction of the carboxyl group of L-serine with His^{159} as depicted in the SPT-PLP-serine crystal structure. Computational study showed that palmitoyl-CoA induced conformational change is related to the displacement of the hydrogen interaction of L-serine with His^{159}: palmitoyl-CoA interacts with His^{159} (hydrogen bond) whereas L-serine performs a new interaction with the guanidine group of Arg^{390} rotating the Cα-N bond of 50°. In this new conformation the Cα-H bond of L-serine is perpendicular to the imine-pyridine plane promoting the α-deprotonation.

The nucleophilic substitution of quinoid intermediate to the acyl-CoA thioester carboxylic group leads to a β-keto-acid derivates. The interaction between palmitoyl-CoA and His^{159} promotes the C-C bond formation by acidic catalysis played by His^{159}: this residue exchange an hydrogen with the carboxylic group of palmitoyl-CoA inducing the right positioning. The product forms an hydrogen bond with His^{159} (the oxygen of the carbonyl group interact with the hydrogen of His^{159}). Then β-keto-acid derivates undergoes to decarboxylation and release of the final adduct (KDS).
Generally PLP catalyzed reactions occur through decarboxylation process catalyzed by the electron withdrawing immine-pyridine system. Instead SPT decarboxylation reaction is promoted by the correct position of the carboxyl group by His^{159}.[1]

4. Inhibitors

Natural inhibitors of SPT have been discovered. Sphingofungine, lipoxamicina (neoenactin M1), and myriocin (ISP-1/thermozymocidin) (Fig.5) are potent and highly selective inhibitors of both fungine and mammals SPT in cell-free models with nanomolar IC50. These compounds are structurally similar to the postulated transitory adduct formed by the L-serine and palmitoyl-CoA during the condensation suggesting the crucial role of a transitory adduct of these compound with PLP in the strong inhibition activity.

Indeed, the inhibitory activity of sphingofungine B is highly dependent on stereochemistry[31,32].

The crucial role of sphingofungine B stereochemistry has been demonstrated: the C14 hydroxyl group of sphingofungine B yields potent inhibitory activity but it's not crucial for the activity. On the other hand, the configuration of the stereogenic centers in the α, β, γ and δ positions from carbonilic group are essential for the inhibitory activity[32,33].

Viridiofungins were first isolated by Harris and co-workers in 1993 from the fungus, *Trichoderma viride*. This family of alkyl citrates exhibited broad spectrum of anti-fungal properties with minimum fungicidal concentrations in the range of 1–20 μg/mL against a number of species. Furthermore, viridiofungins inhibited rat and yeast squalene synthesis. This antifungal activity is unrelated to the inhibition of ergosterol biosynthesis. Instead, viridiofungins showed very potent (nanomolar range) inhibitory activity against serine palmitoyltransferase[34].

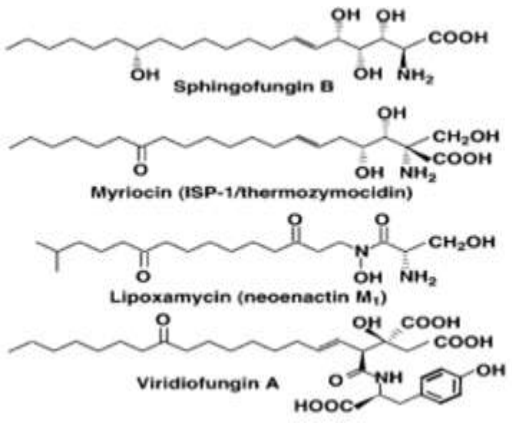

Fig. 5: *Structure of natural SPT inhibitors.*

4.1. Penicillamine

Penicillamine (Pen) is an α-amino acid and a characteristic degradation product of penicillins, used in Wilson's disease as copper chelator to form mixed disulfides with cystein. The enantiomer used as pharmaceutical drug is D-Pen. It has been well established that both enantiomers and racemic mixture exerts anti-PLP activity by inhibiting several PLP-dependent enzymes such as alanine aminotransferase, aspartate aminotransferase, glutamate decarboxylase, hystidine decarboxylase and serine hydroxymethyl transferase. L-Pen has the stronger inhibitory activity thanks to the structure similarity with the enzyme's naturally substrate (L-amino acids) (Fig.6).

Fig. 6: *L-amino acids inhibitors of SPT.*

A recent research developed by Campopiano group, have clarified Pen inhibitory action and mechanism on SPT from *Sphingomonas Paucimobilis* (spSPT). Incubation of D-Pen and L-Pen with spSPT results in different percentage of enzyme inhibition: incubation of 5 mM L-Pen with spSPT reduces enzyme activity to 3% while incubation with D-Pen decreases enzyme activity to 34%. Pen inhibition is reversible and the mechanism of SPT inactivation occurs by disabling the PLP cofactor. Indeed, incubation of enzyme inactivated by D-Pen and L-Pen with a buffer containing 50 μM of PLP, restore the SPT activity to 80% and 57 % respectively. Inability to restore 100% of the activity using a dialyzing buffer is due, probably, to possible additional competitive reactions that irreversibly modify the proteins. The Pen thiol-group plays a crucial role in the inhibition mechanism. The thiol-group is more nucleophilic than the hydroxyl group of the L-Ser and it's able to interact with PLP aldehyde leading to PLP:thiazolidine (PLP:TA) adduct (Fig.7).

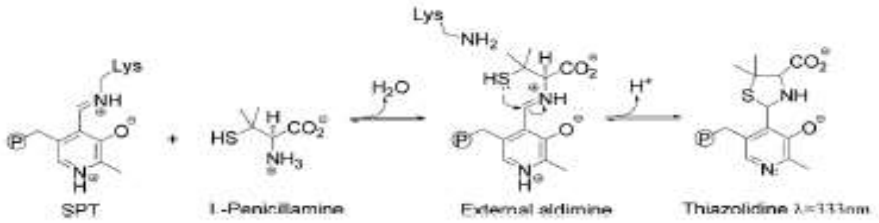

Fig. 7: *Addition of L-Pen to SPT leads to formation of a PLP:TA adduct via an external aldimine intermediate (P represents group phosphate).*

The inhibition reaction could be monitored observing the disappearance of free PLP peaks at 390 nm and appearance of a new peak at 333 nm (thiazolidine adduct). Using the same spectrophotometric approach, a time dependent disappearance of holo SPT ketoenamine (420 nm) and appearance of a thiazolidine adduct have been observed after addiction of L-Pen to holo-SPT. ESI-MS analysis of these samples confirmed the formation of a PLP:TA adduct. Moreover L-Pen and L-cystein activities have been compared highlighting a faster inhibitory activity of L-Pen that could be related to the presence of *gem*-dimethyl group enhancing cycle formation through a Thorpe-Ingold effect[35](Fig.35).

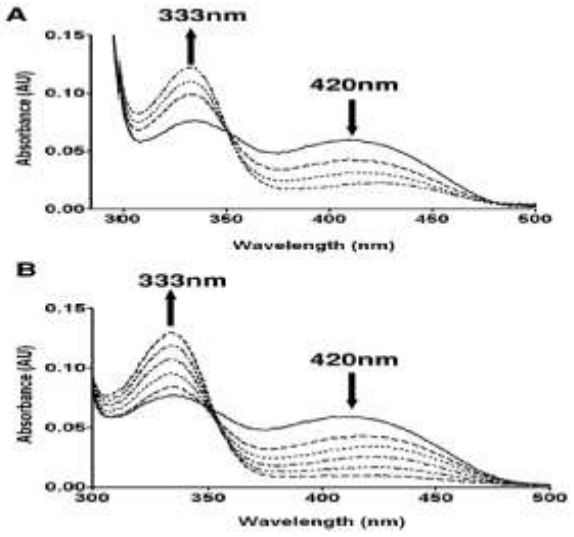

Fig. 8: (A) *UV-visible spectrum of 20 mM holo-SPT (solid line) shows typical peaks at 335 nm and 420 nm due to enolimine and ketoenamine forms of the PLP cofactor respectively. Addition of 10mM L-Cys to holo- SPT (broken lines) led to formation of a thiazolidine adduct (333 nm peak) over a 30 minute period, with concomitant loss of the 420 nm peak* ***(B)*** *improved thiazolidine formation in SPT over 30 minutes by addition of 10 mM L-Pen.*

4.2. Cycloserine

β-chloro-L-alanine and L-cycloserine has been used as SPT inhibitors. These compounds are potent inhibitors of several PLP-dependent enzymes, therefore their use as specific inhibitors is limited[36,37].

Cycloserine (Fig.9a) is cyclic α-aminoacid well known to inhibit many PLP-dependent enzymes (transaminase, racemase and decarboxylase)[38-40]. It exists as two enantiomers: D-cycloserine (DCS) and L-cycloserine (LCS).

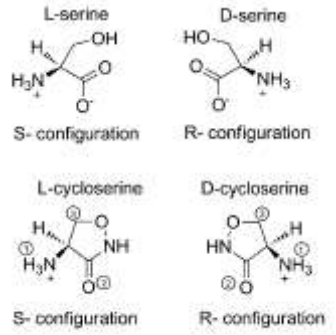

Fig. 9a: "*Conformations" and " structures" of D- and L- α-amino acids inhibitors of SPT.*

The mechanism of antibacterial activity is based on the inhibition of alanine racemase, a PLP-dependent enzyme that synthesize D-alanine for the formation of D-alanyl-D-alanine dipeptide (an essential component of the peptidoglycane layer of the M. tuberculosis)[41]**.** Furthermore, DCS is an agonist of N-methyl-D-aspartic acid (NMDA) receptors that is implicated in several CNS pathologies and it's used in neurological models of these pathologies[42]; LCS has been prepared synthetically and used as a modulator of lipids metabolism in biological research, indeed it is a potent inhibitor of SPT activity. Furthermore, it has been demonstrate that LCS inhibits mouse brain SPT activity *in vivo* after intraperitoneal injection[43]. Some authors propose a cycloserine inhibition mechanism based on aromatization of the PLP:cycloserine external aldimine ("aromatization mechanism") by α-deprotonation that give rise to a 3-hydroxyisoxazole–PMP adduct: the cycloserine ring remains intact and covalenty linked to the PLP.

A first study developed by Ikushiro[44] revealed a change in SPT absorption 10 minutes later the addiction of LCS: the peak corresponding to the ketoenamine tautomer of the internal aldimine (426 nm) decreased whereas a new peak at 380 nm increased. On the basis of this data a mechanism of action was hypothesized: in a first attend LCS reacts with PLP forming and external aldimine that undergoes to decyclization of the isoxazolidone ring (forming a transient oxime intermediate with absorption at 380 nm) leading to pyridoxamine 5'-phosphate (PMP) and β-aminooxypyruvate (Fig.9b).

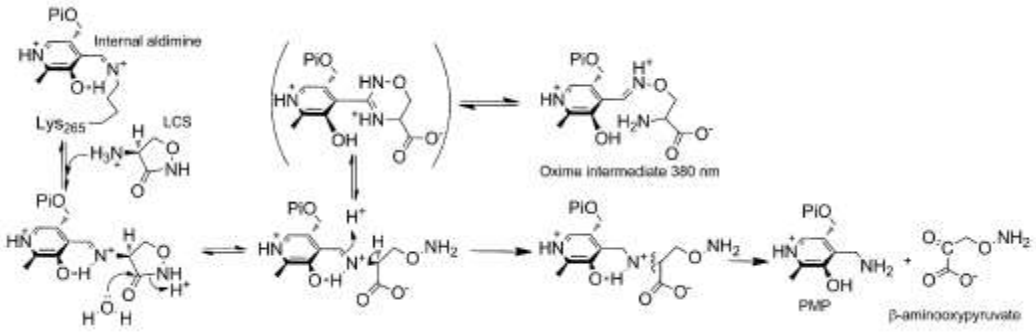

***Fig. 9b**: Proposed mechanism of LCS inactivation of SPT by Ikushiro et al.*

In 2010 the research group of Campopiano[45] have highlighted the enantiospecific inhibition of LCS and DCS and they have identified a novel decarboxylative ring-opening mechanism for inactivation of SPT. In particular the data show that in order to obtain the same inhibition of SPT activity (to the same extent and over the same time) 15-fold higher concentration of DCS is needed in comparison with LCS showing a clear enantiospecific difference of the enzyme active site (Fig.10).

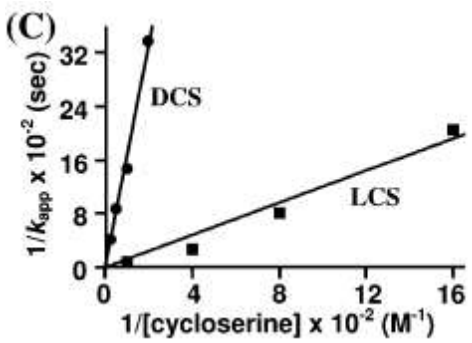

Fig 10: Secondary plot of $1/k_{app}$ versus 1/[inhibitor] for LCS and DCS.

SPT activity (monitored by continuous DTNB assay) is reduced to 1% and 22 % after 2 hours incubation with 5 mM of DCS and LCS respectively. Furthermore incubation of treated samples in a buffer containing 25 μM of PLP caused the recovery of SPT activity (83 % and 79 % of DCS and LCS inactivated samples respectively). Incubation of the inhibited enzyme in buffer (without PLP) doesn't cause any further change of activity (the enzyme is still inactivated). These data confirm the disabling of PLP activity and the absence of further covalent modifications occur. The incubation of enzyme with DCS and LCS showed different UV-spectra. After 30 minutes from the addiction of 5 mM LCS new peaks appear at 330 and 380 nm and no more changes were observed when the incubation time was about 8 hours. Incubation of DCS with SPT causes the loss of the 425 nm peak and the appearance of a new peak at 380 nm. This peak shifted to 365 nm over time and at the same time a broad shoulder at 330 nm appeared (Fig.11A). These results suggest the formation of different species and the displace of the new PLP-Lys^{265} bond. In contrast, the UV-VISis spectra of free PLP in the presence of both enantiomers show the same peak at 360 nm (Fig.11B).

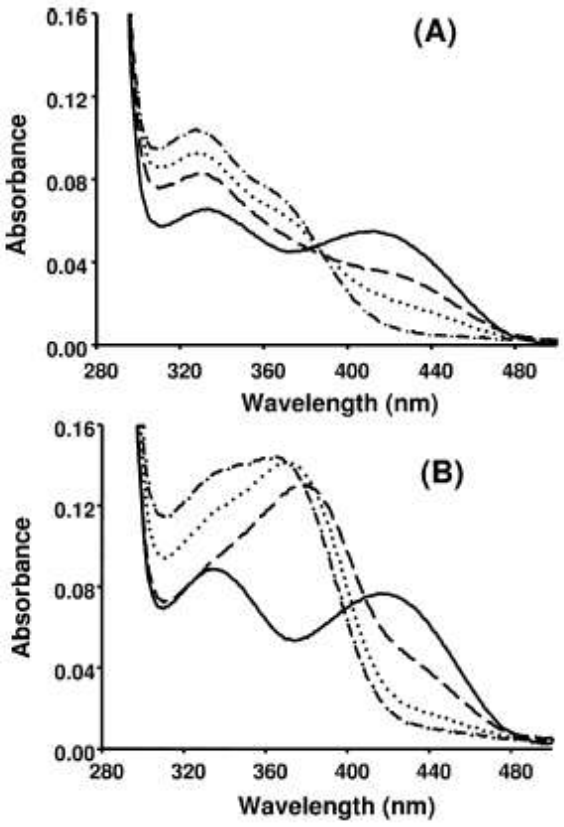

Fig. 11: (A) *SPT and 5 mM of LCS at time 0 (solid line), 30 seconds (long dash), 1 minute (dotted line) and 30 minutes (dash dot).* ***(B)*** *SPT and 5 mM of DCS at time 0 (solid line), 30 seconds (long dash), 2 hours (dotted line) and 10 hours (dash dot).*

This last one result suggests that enzyme not only accommodate the PLP-cycloserine aldimine adduct but it's also implicated in the formation of new different species.

The reaction intermediates have been identified by LC ESI-MS analyses of SPT samples incubated with LCS: a peak at 2.8 minutes (m/z = 248) corresponding to PMP and another peak at 3.1 minutes (m/z = 256) corresponding to [M + H] ion of a hydrazine adduct formed by the derivatisation of the β-aminooxyacetaldehyde with 2,4-dinitrophenylhydrazine (2,4-DNP) have been identified. These peak wasn't observed in control experiments with free PLP and 2,4 DNP derivative. These results suggest that the mechanism of LCS inhibition is based on the ring-opening of LCS by cleavage of the amide bond: this phenomenon take place because the C-α proton in the PLP:LCS external aldimine cannot be in the optimal orientation to be removed by the lysine. Successively two different decarboxilative pathways can take place: a) the ring-opened intermediate is acylated (enzyme mediated mechanism) and hydrolysed to form the carboxylated PLP intermediate (path [a] Fig.12); b) ring-opened adduct could proceeds through acid catalysis with water nucleophilic attack on the CS ring (path [b] Fig. 12).

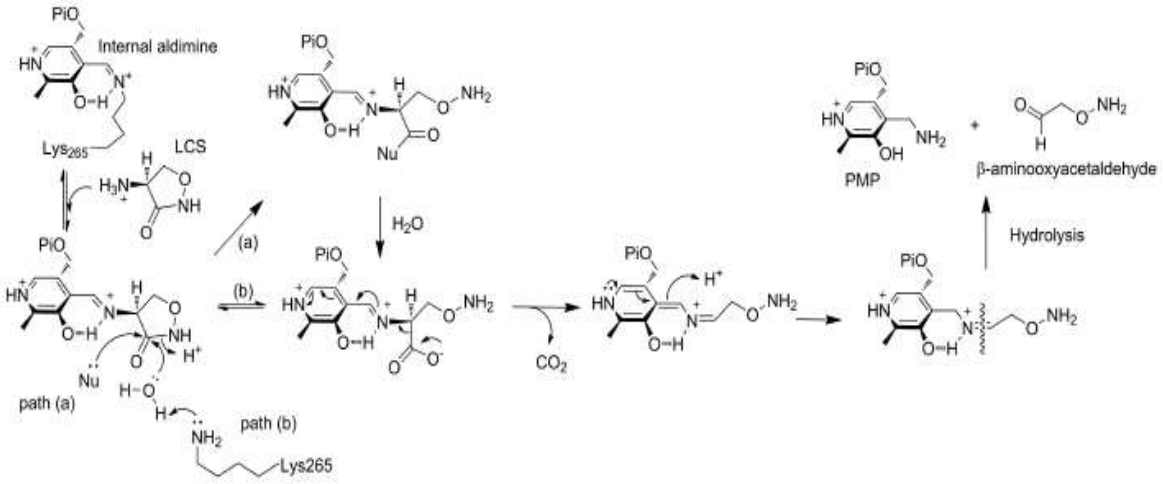

Fig. 12: *Novel ring-opening, decarboxylative mechanism for inactivation of SPT by LCS. Path (a) denotes an enzymatic, nucleophile (Nu)- mediated mechanism with an acylated intermediate. Path (b) is the direct hydrolytic mechanism.*

These pathways may come to form an oxime intermediate (observed as a 380 nm peak in the UV-visible spectrum) or decarboxylated adduct that is followed by the hydrolyzed immine form which conduct to PMP and β-aminooxyacetaldehyde .

Using a SPT R378N (a mutant which contain in the active site an alterated Arg^{378} residue that form a salt bridge with the carboxylate of the external aldimine) permit to

isolated intermediate and 40 fold reduced rate when compared with the wild-type enzyme, it was observed transient formation of a quinonoid species (formed by decarboxylation) at 510 nm during DCS inactivation, while inactivation with LCS (much faster inactivator in comparison with DCS) show a similar spectrum to the wild-type enzyme at 380 nm[45].

In addition these researches has been conducted with modeling to isolated the PMP adduct (Fig.13).

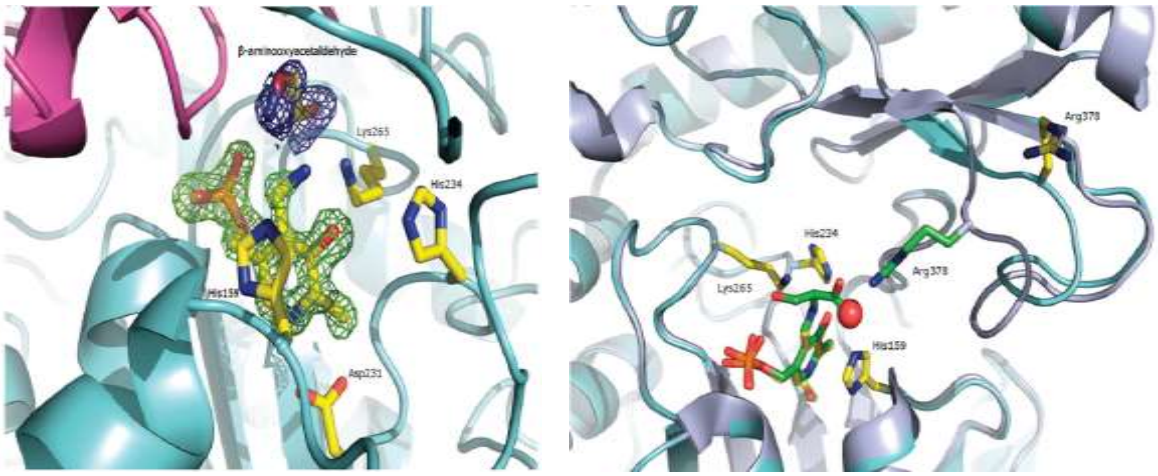

Fig.13: ***<u>Left:</u>*** *Fo-Fc electron density for the PMP molecule. This was calculated from molecular replacement model which was refined and had omitted the co-factor. The map is contoured in green at 3s (0.2 Å^3). Also shown are the side chains of Lys265, His159, Asp231 and His234. Monomer A is shown in ribbon in cyan and monomer B in magenta. The additional Fo Fc electron density ''blob'' is shown in blue, contoured at 2.7s (0.2 Å ^{3}). A molecule of the β-aminooxyacetalaldehyde identified by mass spectrometry is placed in the density. Carbons are colored yellow, nitrogen blue, oxygen red and phosphorous orange.* ***<u>Right</u>****: Overlay of SPT:L-ser (2bwj) and the LCS inactivated form. The loop containing R378 adopts the ''swung-out'' conformation in the LCS form, in contrast to the ''swung in'' conformation in SPT:L-ser. The color scheme for the LCS inhibited form is as (left). For the SPT:L-ser structure, monomer A is colored light blue. Carbons are colored green, and other atoms are colored the same as in (left). The main chain of R378 adopts a very different conformation from the SPT:L-ser structure because the salt contact with L-ser is missing. A well-ordered molecule (red sphere) in the LCS structure is found in the same location as the L-ser carboxylate. The side chain of L-ser points towards the unfitted blob at the active site.*

4.3. Myriocin

Natural products and their derivatives are known to be excellent tools for biochemicals and pharmacologicals studies. Myriocin [(2S, 3R, 4R, 6E)-2-amino-3,4-dihydroxy-2-(hydroxymethyl)-14oxo-6-eicosenoic acid] (Fig.14a) also known as thermozymocidin and ISP-1, has potent immunosuppressant properties in addition to antibacterial and antifungal activity.

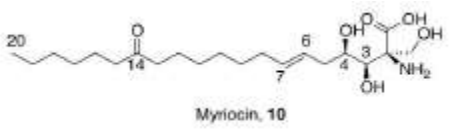

***Fig. 14a**: myriocin structure*

Firstly isolated by thermophilic moulds *Myriococcum albomyces* and *Mycelia sterilia*, myriocin remains the most valuable and widely used chemical probes in sphingolipids research as demonstrated by several studies: the identification of the two SPT subunits (SPTLCB1 and SPTLCB2) by Screiber *et al.*[27] and of multi-protein membrane-bound SPT complex (SPOTs complex) by Breslow *at al.*[28] has been performed using myriocin. Kawasaki and collagues determined an IC50 value of 15 nM using cytotoxic T-cell line (CTLL-2)[46]. Moreover, a recent study has demonstrated that myriocin reduces ceramide levels in rd10 mouse model of retinitis pigmentosa (RP) and therefore can rescue photorecepetors death[47]. Despite its use, the molecular basis of myriocin inhibition of SPT is largely unknown. Campopiano and coworkers have recently shed light in molecular mechanism of SPT inhibition by myriocin using a soluble and recombinant form of the enzyme from *Sphingomonas paucimobilis* (spSPT). Uv-vis analyses after addition of five-fold molar excess of myriocin to holo-SPT revealed that the two characteristic peak at 333 nm and 420 nm (corresponding to the ketoenamine and enolimine forms of the external aldimine) led to an increase absorbance with maximum at 430 nm and the disappereance of the peak at 333 nm. This data reflects a transamination reaction between PLP and myriocin that lead to the formation of a stable an external aldimine mimicking the β-keto acid intermediate, Fig.14b and confirmed by LC ESI-MS analyses Fig.14.b-B.

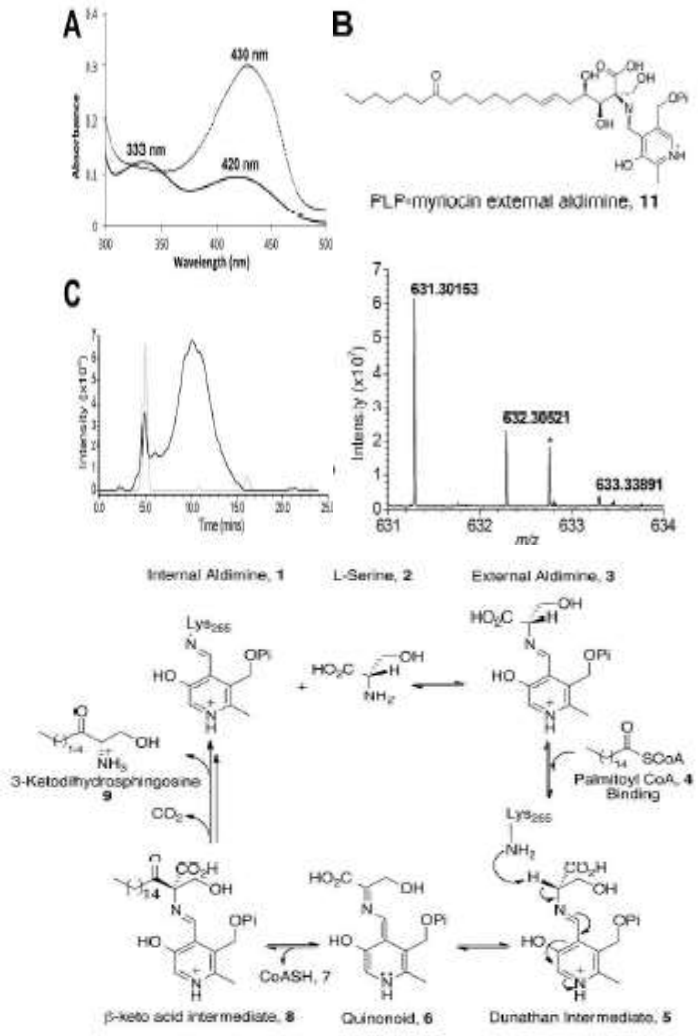

Fig. 14b: *SPT inhibition occurs via formation of a PLP-myriocin aldimine.* ***(A)*** *UV-Vis spectrum of 40 μM SPT before (solid line) and after 200 μM myriocin addition (dotted line).* ***(B)*** *The proposed structure of the inhibitory complex - a PLP-myriocin aldimine,* ***11****.* ***(C)*** *Detection of the PLP-myriocin aldimine by LC-MS. Top, Extracted Ion Chromatogram at m/z 631. Bottom, high resolution mass spectrum of the PLPmyriocin aldimine, obtained by summing the spectra between t = 8-12 minutes. ($[M+H]^+$, $C_{29}H_{48}N_2O_{11}P$; predicted m/z 631.29902; observed error 4.0 ppm). * denotes a contaminant.*

Interstingly PLP-myriocin aldimine (**11**) is relatively stable at 25°C. However, after 16 hours of incubation a decrease of 430 nm peak and increase of 331 nm and 400 nm peaks is revelead (Fig.15).

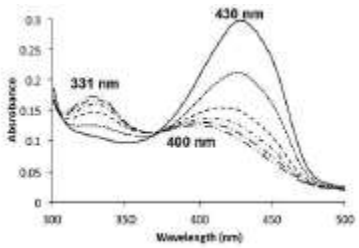

Fig.15: *UV-vis analysis of the degradation of the PLP-myriocin external aldimine in wild-type SPT. The PLP-myriocin external aldimine (solid line) is stable for 90 minutes, before a decrease at 430 nm is observed, which is accompanied by a concomitant increase at 331 and 400 nm over 16 hours (dotted and dashed lines).*

SPT:PLP-myriocin complex has a noncovalent, reversible nature and very slow off rate (k_{off}) when incubated with myriocin for 10 minutes: sample dialysis in 25 μM PLP containg buffer for 24 hours restored enzyme activity of 60% (accompanied with UV-Vis spectrum back to the internal aldimine). On the other hand a covalent and irreversible nature of myriocin-enzyme interaction has been observed when samples were incubated for 16 hours (Fig.16). Moreover, experiments demonstrate that myriocin is a competitive inhibitor for both L-serine and palmitoyl-CoA and a Ki of 967±98 nM.

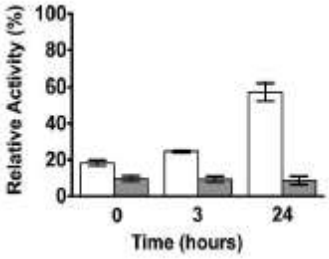

Fig.16: *Relative enzymatic activity after removal of inhibiting species by dialysis. SPT was inhibited with 200 μM myriocin and incubated for 10 minutes (white bars) or 16 hours (grey bars) at 25 °C before removal of myriocin by extensive dialysis. The enzymatic activity was then determined at 0 hours, 3 hours, and 24 hours after dialysis.*

To better understand the role of the Lys 265 in the dual reaction mechanism of myriocin, an incubation with five-fold molar excess of myriocin and catalytically-inactive SPT (K265A SPT) which present active site without Lys residue was performed. After 16 hours the UV-Vis spectra remained unchanged in contrast with wild-type SPT suggesting that the initial SPT:PLP-myriocin inhibitor complex breaks down to form a second species that also inhibits wild-type SPT (Fig.17).

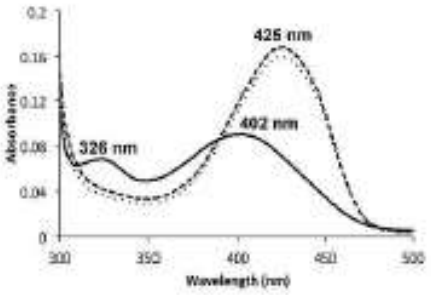

Fig. 17: *UV-vis analysis of SPT K265A (40 μM) showed two absorbance maxima at 326 and 402 nm (solid line). Upon addition of 200 μM myriocin, an immediate shift to a single peak at 425 nm occurred (dotted line), indicating the formation of a PLP-myriocin aldimine complex. Over 16 hours this spectrum remains unchanged (dashed line), indicating that the PLP-myriocin aldimine complex is not degraded by this mutant enzyme.*

A retro-aldol like mechanism of SPT:PLP:myriocin complex which selectively and covalently modifies the Lys^{265} (crucial for the enzyme-catalysed reaction) leading to irreversible inactivation of the enzyme was hypothesized (Fig.18).

Mass spectrometry analyses showed a covalent adduct (14 in Fig.18) of SPT displaying a mass of 47.509 Da susceptible to $NaBH_4$ of the covalent SPT-octadecenal imine adduct and ketone group. Peptide mass fingerprinting identified Lys^{265} as the site of modification. Trypsin digest and mass spectrometry analysis identify three peptide species which displayed monoisotopic masses consistent with Lys^{265} modified by Δ mass +282.24 (Fig.19).

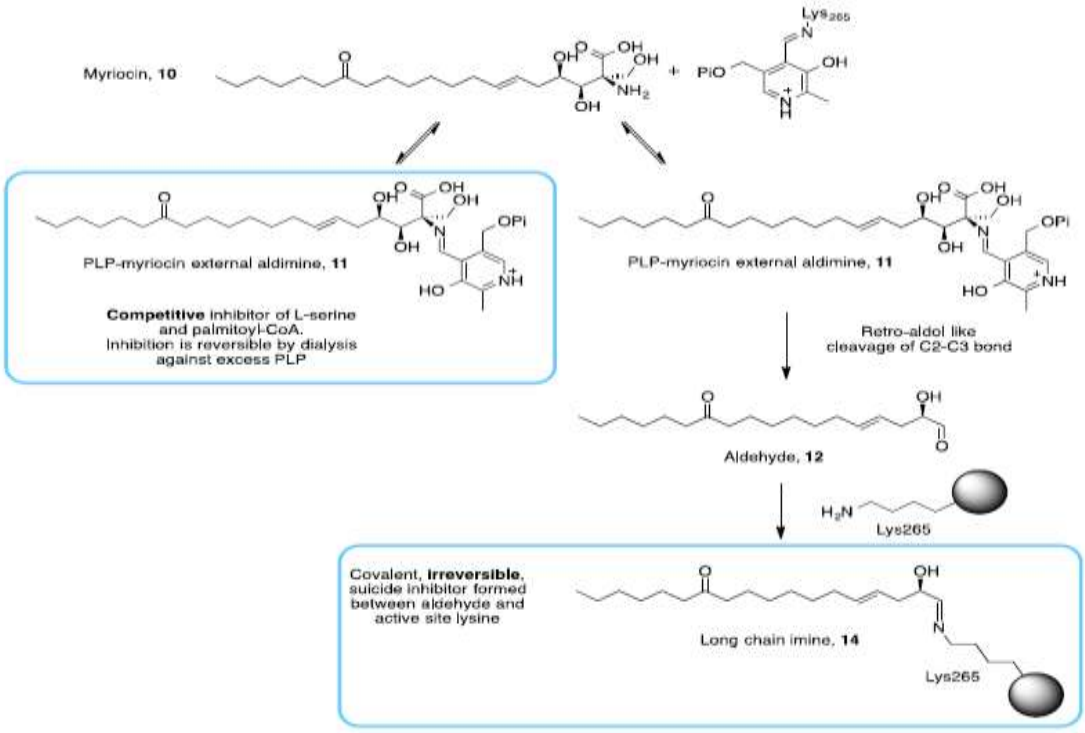

Fig. 18: *Myriocin reacts with PLP in the active site to form the inhibitory PLP-myriocin aldimine* ***11****, this species is stable for greater than an hour at physiological temperature with inhibition being reversible upon addition of excess PLP.*

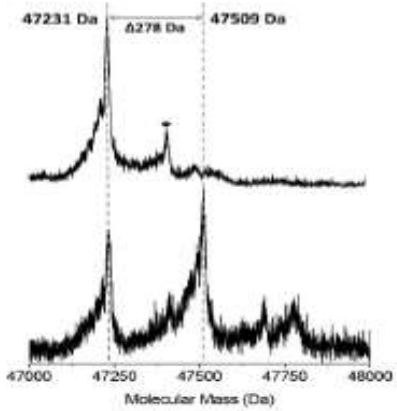

Fig. 19: *PLP-myriocin aldimine* ***11*** *(Fig.18) decomposes over 16 hours, at physiological temperature, to produce a long chain aldehyde* ***12*** **(**Fig.18*) that react with the active site lysine to form an imine, thus rendering the enzyme inactive. This covalent modification can be classed as suicide inhibition.*

Due to the timescale of crystallization, the PLP-myricin aldimine degrades into the wilde-type enzyme and catalytically inactive K265A has been used to capture external aldimine which results stable and decompose only after seven days with a decarboxylation reaction. This slowness relative to wild-type complex is due to the not optimal orientation ("Dunathan conformation") suggesting the crucial role of the Lys^{265} in the decarboxylation of the SPT:PLP-myriocin complex (Fig.20).

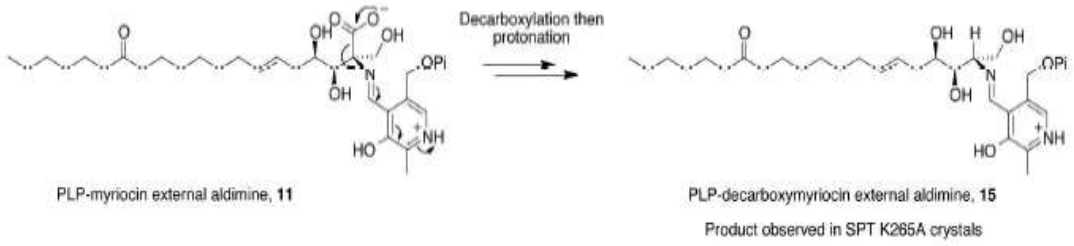

Fig. 20: *Decarboxylation mechanism to account for PLP-decarboxymyriocin external aldimine observed in the crystal structure of SPT K265A.*

The crystal structure obtained highlights that the conserved residues His^{159}, Asp^{231} and His^{234} are all in the same relative positions within the active site. Moreover, the CH_2OH head group of myriocin interacts with the 5′-phosphate of PLP. The 3,4-*cis*-diol of decarboxymyriocin makes hydrogen bonds to the protein, notably the 3-hydroxy group of myriocin with the important catalytic residue His^{159}; this interaction would be expected to be preserved in the wild type SPT:myriocin complex. The hydrogen bond network that surrounds and includes the 4-hydroxy group of decarboxymyriocin may be changed by the presence of Lys^{265} but at least some of the same network seems certain to persist and this too involves the same residues that interact with the carboxylate of the PLP-L-serine external aldimine. These interactions rationalize the competitive inhibition with L-serine. Accompanying these interactions are movements of the side chains of Tyr^{73}, Arg^{378} and Arg^{390} as well as a displacement of a key conserved stretch of amino acids (RPPATP) that constitute a mobile loop that undergoes conformational changes during the catalytic cycle. The 6,7 *trans* double bond geometry of myriocin is clearly defined and we can see electron density for the carbon chain up to C9 which sits in the hydrophobic cleft adjacent to PLP. The carbon tail of myriocin binds in a similar orientation to the decanoyl-tail of the PLP-product external aldimine observed bound in the crystal structure of the related AOS enzyme CqsA from *Vibrio cholera* consistent with hypothesis that myriocin mimics the condensation intermediate (Fig. 21).

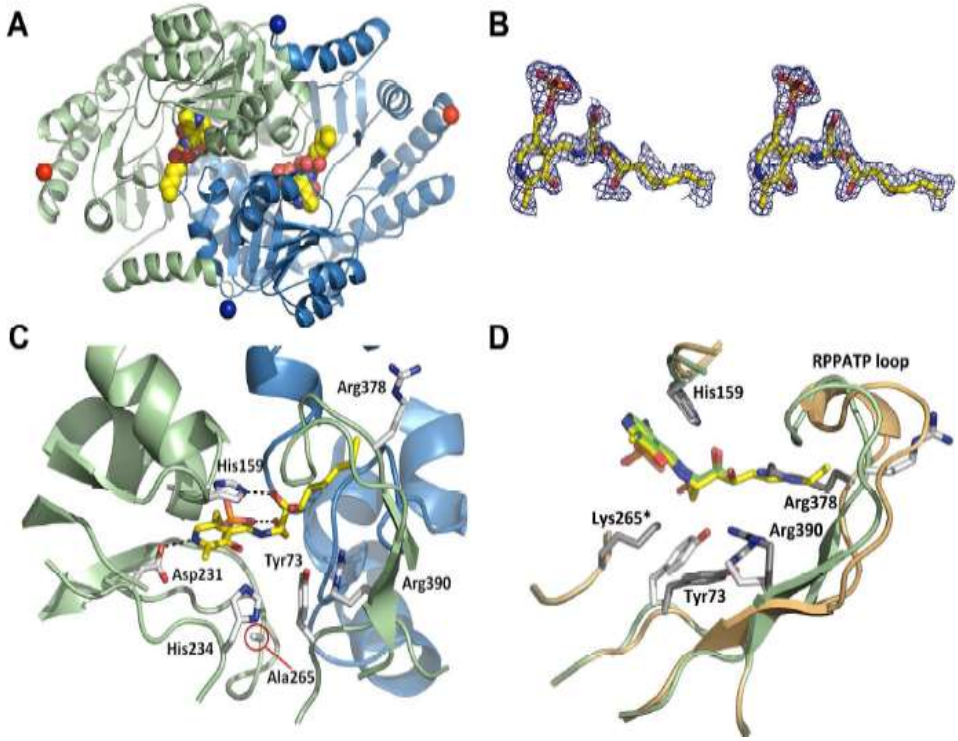

Fig. 21: *The structure of SPT K265A PLP-decarboxymyriocin aldimine inhibitory complex.* ***(A)*** *The biological SPT dimer of the decarboxylated myriocin complex. The protein is shown as a cartoon with one subunit colored pale green and the other pale blue. The PLP external aldimine of the decarboxylated myriocin (**15**) is shown in space fill with carbons colored yellow, nitrogen blue, phosphorous orange. The N terminii are marked as dark blue spheres and C-terminii as red spheres.* ***(B)*** *Left, The Fo-Fc map (blue chicken wire contoured at 1.8σ, carve radius 1.5A) calculated from a model which had never contained either PLP or myriocin. Atoms are colored as figure 6A. Right, the final Fo-Fc map contoured at 0.85σ with a carve radius 1.8 Å.* ***(C)*** *Detailed representation of the active site interactions, carbon atoms are colored yellow and shown in sticks for the PLP-decarboxymyriocin aldimine **15**. Carbon atoms in protein side chains are shown as white sticks, others atoms are colored as figure 6A. The hydrocarbon chain of the myriocin inserts into a hydrophobic pocket.* ***(D)*** *Superposition of the PLP-decarboxymyriocin external aldimine (colored as before) with the PLP-L-serine external aldimine 2W8J (cartoon pale orange, protein side chain carbons dark grey, aldimine carbons colored green, other atoms are colored as before). The key catalytic Lys265 residue is mutated to Ala in the decarboxylated myriocin complex.*

This structure rationalizes the retro-aldol degradation of the PLP-myriocin external aldimine **11** into corresponding to the C18 aldehyde **12**. This mechanism requires a base to abstract the proton from the 3-hydroxy group of myriocin but Lys^{265} would be in wrong face to perform this role. However, the absolutely conserved His^{159} is positioned 2.6 A away from the 3-hydroxy of myriocin and probably initiates the cleavage of the C2-C3 bond with the electrons sinking into the PLP ring. In the other hand deprotonated Lys^{265} is positioned to attack the newly formed C18 aldehyde species **12** to form a covalent aldimine adduct **14** and modifies the key catalytic lysine residue irreversibly and block access to the active site preventing regeneration by PLP on a biologically-relevant timescale[46].

5. Retinitis Pigmentosa

Retinitis pigmentosa (RP) is a general term related to a wide range of rod and cone dystrophies characterized by progressive night blindness, visual field constriction and loss of acuity leading to an altered electroretinogram (ERG)[48]**.** Currently, there is no therapy able to stop the disease's evolution based more frequently on mutations of genes involved in rod photoreceptors function and metabolism. Rods and cone photoreceptors cells death occurs through both apoptotic and non-apoptotic mechanisms[49].

In many neurodegenerative and inflammatory diseases, an increase of the intracellular levels of ceramide, a well-characterized death effector, has been revealed. A direct genetic link between retinal degeneration and sphingolipid mediated apoptosis has been highlighted by the discovery of a mutation in CERKL (a gene expressing ceramide kinase-like protein) which causes loss of function and autosomal recessive RP[50].

Ceramide levels are increased by *de-novo* biosynthesis or by activated intracellular sphingomyielinase which hydrolyze complex sphingolipids leading to ceramide. The *Drosophilla* model of RP *(knock out* of the gene encoding for one subunit of SPT) is characterized by a decrease of ceramide intracellular levels and protective effects in retinal function and morphology. Also the injection of ceramidase, a ceramide hydrolyzing enzyme, results in a decrease of ceramide intracellular levels and protective effects[51]**.** In the murine 661W photoreceptor cell line, oxidative stress can increase ceramide levels leading to cell death via mitochondrial apoptotic pathway activation and caspase cascade[52]**.** Therefore, inhibition of ceramide biosynthesis, accordingly with biochemical analyses, may represent a therapeutic approach for the treatment of this disease in humans.

A useful model for human RP is represented by rd10 mice line[53] which presents a missense mutation of the beta subunit of the rod-specific phosphodiesterase gene, and mimics a form of human autosomal RP. Rd10 mice retinal ceramide levels increased at the third week of life, which correspond to the maximum photoreceptor death period as well as the human RP. These high levels are constant for the following period, whereas in wild-type mice ceramide levels decrease during the same period reaching a plateau after full retinal maturity. Rod death starts about at 12 days of life (P12) and reach the maximum peaks at 24 days of life (P24). Indeed ERG (electroretinogram) generated by

rods can be recorded up to 25 days of life (P25) until 45 days of life (P45) due to death of the retinal cones. Rod degeneration presents the characteristic features of apoptosis[54]. In rd10 mice model of RP, single intraocular injections of 0.5 nmol (1 μL of 3.77 mM solution in DMSO) of myriocin, significantly decrease ceramide levels (17.5%) than in control, and rescued photoreceptors from apoptotic death whereas the ceramide levels in wild type are not significantly reduced (determined with the diacylglycerol kinase test). Eye drops consisting in a suspension of solid lipid nanoparticles (SLNs) loaded with myriocin, carried the drug across ocular tissues permitting trans-ocular drug administration: the non-invasive and long term treatment of these drops ameliorate the reduction of function loss and of ceramide levels (40.6%). Histological analyses (Fig. 22) demonstrate that myriocin treated rd10 mice presents normal retinal morphologies and excellent maintenance of ganglion cell morphology and structure: prolonged treatment (over 20 days) with solid lipid nanoparticles increase photoreceptor survival, preserving photoreceptor morphology (rhodopsin and cone immunoreactivity in well-organized outer segments of rods and cones and presence of well-organized dendrites in rod bipolar cells) and extends the ability of the retina to respond to light (demonstrated by the ERG)[55]**.** These data highlight that SPT inhibitors could be an useful tool for the treatment of RP**.**

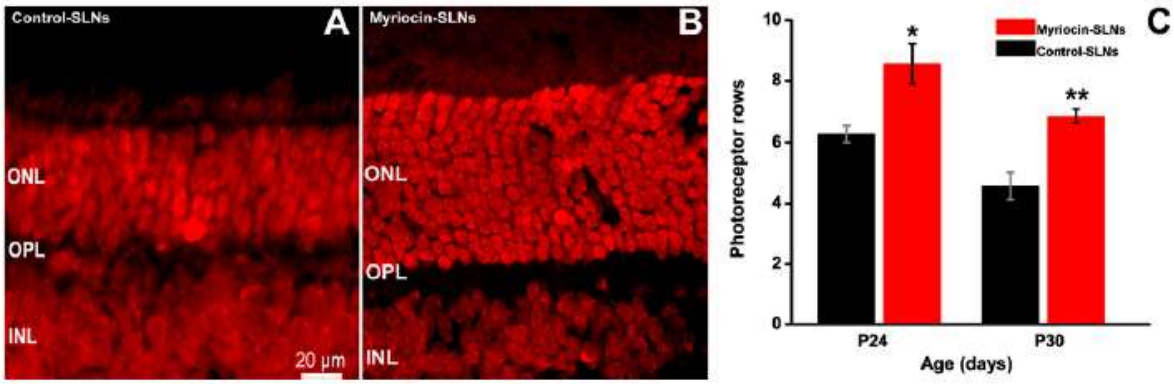

Fig. 22: *Effects of myriocin-SLNs on retinal morphology. (**A** and **B**) Vertical retinal sections from rd10 mice treated with control SLNs **(A)** andmyriocin-SLNs **(B)** for 10 d (from P14 to P24). The outer nuclear layer (ONL) of the myriocin-treated retina is thicker because it contains more photoreceptor rows than the control retina. These micrographs are from the same animals whose ERG data are shown in Fig. 4B. INL, inner nuclear layer; OPL, outer plexiform layer. **(C)** Quantification of photoreceptor rows at P24 and P30 in rd10 mice treated with control SLNs or myriocin-SLNs. Data are mean and SE. *P = 0.002, **P = 0.003, t test.*

6. Alzheimer

Alzheimer's disease (AD) is the most common form of dementia. It was firstly described in 1906 by the german neuropathologist Alois Alzheimer. AD is characterized by short-term memory impairment, language disturbance (aphasia), confusion, irritability and loss of both judgment and reasoning ability, including deficiency of acetylcholine. The anatomical consequence of the cholinergic deficit is the atrophy and degeneration of subcortical cholinergic neurons (especially in the basal forebrain). This brain region provide cholinergic innervation to the cerebral cortex involving multiple neurotransmitter systems, including serotonin, glutamate, and neuropeptides. Not only cholinergic neurons are involved in AD, cortical and hippocampal targets are also interested. In the early stages (clinically silent stages) neurons degeneration and plaques formation in the hippocampal cortex take place and in late stages limbic and neocortical sites (conclamated AD) are involved.

Microscopic analyses of the affected parts of the brain have demonstrated the presence of a large amount of intracellular neurofibrillary tangles (NFT) consisting in microtubule-associated protein tau in the hyperphosphorilated and insoluble form. Moreover there are extracellular amyloid in the form of senile plaques (SP) consisting of a core of amyloid β-peptides (Aβ). For that reason AD represent one of the 20 clinically defined amyloidosis disease. The severity of impairment is roughly proportional to tangles and plaques abundance. The observed deposited fibrils were in a misfolded form β-sheet called β-amyloid**.** These components appear elevated in the hippocampus and in the associative regions of the cortex. Indeed, neural injury is most severe in the hippocampus and neocortex. Astroglia and hippocampal neurons exposed to β-amyloid show characteristic changes of apoptosis. The loss of neurons is not uniform but it varies dramatically in relation to functional regions. Mutations in the genes encoding for the amyloid precursor protein (APP), a type 1 cell surface glycoprotein which has neurotrophic and neuroprotective activity, and proteins known as the presenilins (PS1 and PS2), which may be involved with secretases (α, β and γ) enzyme in APP processing, lead to the formation of the Aβ. The presenilins and their mutated forms (in the PS1 gene on chromosome 14 and in the PS2 gene on chromosome 1) participate in APP processing leading to production, among others, of 4-kDa β-amyloid peptide of varied amino acid lengths, predominantly 40-42 (called $A\beta_{40}$ and $A\beta_{42}$ respectively). The production of Aβ from APP appears to result from alterated

proteolytic cleavage of APP by the β-site APP-cleaving enzyme 1 (BACE 1)[56-60]. Apolipoprotein E (apo E) has been identified as the first of what are likely to be many genetic risk factors for AD, involved in transport of cholesterol and lipids in blood. The mechanism by which the apo E 4 protein increases the risk of AD is unknown, but a secondary function of the protein in β-amyloid aggregation or processing of APP has been suggested. Lipid metabolism and high fat diet are risk factors for AD. Indeed, adequate intracellular ceramide is required for dendritic differentiation and survival of Purkinje cells[61,62] while exogenous ceramides induce neurons and astroglia death in culture[63-66]**.** Elevated ceramide levels are show to be a risk factor for AD[67-71]. Significant increase of the death-effector ceramide has been observed in AD patients neurons exposed to Aβ compared with control suggesting a molecular interaction between these two species. Aβ accumulation may cause oxidative stress as demonstrated by increased levels of the lipid peroxidation product 4-hydroxynonenal (4-*HNE*) in neurons exposed to Aβ[72-74] and alteration of membrane lipid metabolism increas ceramide and sphingomielyn levels; this phenomen lead to synaptic function alteration, degeneration and neurons death (Fig.23). Moreover, alteration of the ceramide and cholesterol metabolism increases the γ-secretase's cleavage of APP and enhances the production of $A\beta_{42}$[75].

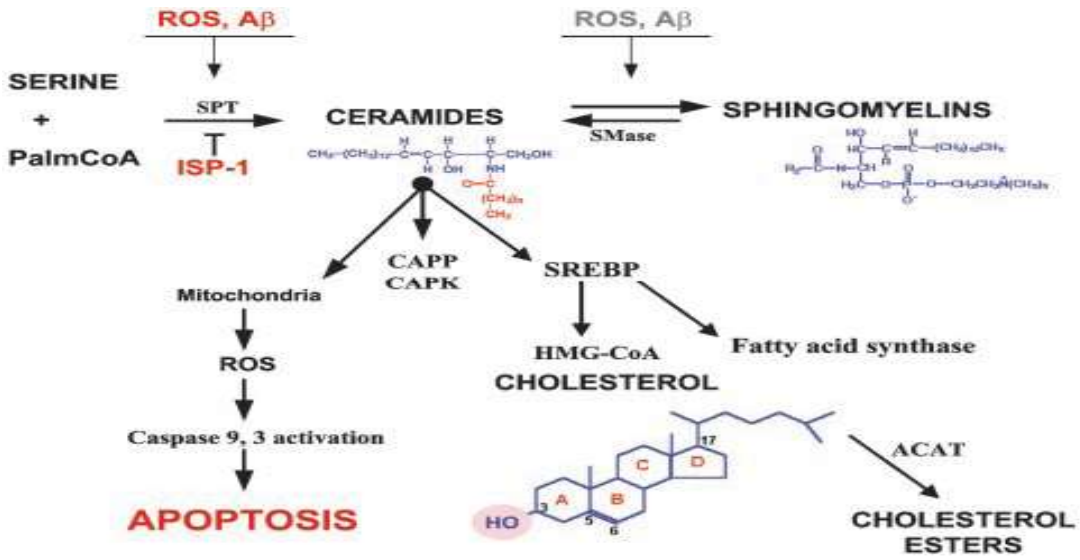

Fig.23*: Pathways of metabolism of sphingomyelin, ceramide and cholesterol, their modulation by oxidative stress, and their possible roles in neuronal death in AD. The production of sphingomyelin from serine and palmitoyl CoA is catalyzed by the enzyme serine palmitoyltransferase (SPT). Ceramides are synthesized as precursors to sphingomyelin and are also generated by the hydrolysis of sphingomyelin by sphingomyelinases (SMase). Exposure of cells to reactive oxygen species and Aβ induces ceramide production. CAPK, ceramide-activated protein kinase; CAPP, ceramide-activated protein phosphatase*

In pathological conditions, ceramide facilitate the mislocation of BACE 1 and γ-secretase from outside to the lipid rafts, where secretase cleavage of APP leading to the Aβ. Membrane ceramide stabilize BACE 1 affecting the activity of the γ-secretase[76-80]. Moreover, SPT appear increase and positively correlates with Aβ in human autopsy brain cortices, directly regulates their concentration in the serum and brain. Utilizing wild-type hybrid mice (C57/Bl6 x C3H), during a high-fat-diet of 5 months (starting at 4 months age) it was show an increase of SPT levels whereas in the same model a high-fat-diet of 3 months has not showed the same increase suggesting that the duration of high-fat diet consumption could have effect on metabolic processes[81].

Also in these studies L-cycloserine (LCS) has demonstrated *in vitro* and *in vivo* reduction of cerebroside levels which largely consist in ceramide with polar head and single glucidic residue[82]. Furthermore, cognitive enhancement has been observed in AD patients in a duble-blind controlled trial with treatment of cycloserine (100 mg/day for 14 days)[83]. In an early-onset transgenic mice model, TgCRND8, encoding a double mutant form of APP 695 (KM670/671NL1V717F) under the control of the PrP gene promoter[84], LCS has demonstrated to reduce $A\beta_{42}$ ceramide levels in comparison with mice fed a high fat diet and also in comparison with mice fed a control chow diet. LCS administration cause a decrease of cortical SPT protein levels with a significant positive correlation with ceramide and $A\beta_{42}$ levels in all the study groups. Furthermore, SPT appear to surround the SP in TgCRND8 mice and humans supporting the involvement of the enzyme in the Aβ formation. Moreover, LCS cause a decrease of the hyperphosphorilated tau protein reducing levels GSK3b (a kinase that mediates phosphorylation of tau). The administration of large doses (100 mg/kg) of LCS reduce immediately brain SPT levels with weight loss while low dose (25 mg/kg) show side effects without weight loss. Chronic LCS (by an intraperitoneal surgically implanted osmotic pump) administration doesn't change brain histology, morphology, myelination, or memory in healthy mice with the LDH serum levels unchanged[85].

7. Hereditary Sensory Neuropathy Type 1 (HSAN 1)

HSAN 1 is a neuropathy characterized by loss of pain, temperature sensation in hands and feet accompanied with skin ulcers, infections and high pain[86]. In addition, degeneration of motor neuron occurs with consequent atrophy and weakness of distal muscles of hands and legs[87,88]. Today it has been identified missense mutation at the SPTLC1 gene encoding the first subunits of SPT[89-91]. Analysing 24 HSAN1 families patients, four missense mutations have been reported corresponding to C133W, C133Y, V144D, and G387A but recently have been reported two others mutations associated with HSAN 1. The most frequent mutation observed is an C133W, while G387A is a relatively not common mutation and doesn't look like disease-causing mutation[92]. Heterozygous SPTLC1 and SPTLC2 knock-out mice doesn't develop the neuropathy. This data changed the common think that HSAN 1 is due to a loss of SPT function and haploinsufficiency should be reflected in reduced total sphingolipid levels. Indeed, the total sphingolipids levels are not increased in SPTLC133W transgenic mice that develop an age-dependent peripheral neuropathy with motor and sensory impairments[93]. Cells can also generate ceramide by the degradation of sphingomyelin from external sources and therefore they are principally able to compensate reduced *de novo* ceramide synthesis[94]. To analyze total sphingolipids levels and the correlation with *de novo* synthesis of ceramide, it has been utilized the SPT inhibitor myriocin and the ceramide synthase (CerS) inhibitor fumosin B1 (FB1) which lead to accumulation of sphingolipids (permitting to observe the type of sphingolipids accumulated). In the HEK133W and HEK133Y expressing the SPTLC 1 mutant line cell, result in 50% reduction of the sphingolipids levels utilizing FB-1 in comparison to wild-type cell not expressing the SPTLC1 mutant. Furthermore, presence of unusually peak in cell lines expressing the mutant SPTLC1 but not in the wild-type line cells have been revealed. This peak disappears of cell lines treatment with myriocin suggesting direct correlation between SPT and the peak revealed in mutant cell lines. When extracted and analyzed the peak revealed two different metabolites with mass to charge ratio (*m*/*z*) of 462.3 and 448.3, these correspond to 16 and 30 Da smaller than sphiganine (SA); *m*/*z*=478.3) with loss mass of oxygen (16 Da) or hydroxymethyl group (30 Da), respectively. Several analyses reveal that these metabolites have a sphingoid backbone with lack of the hydroxyl group at the C1 therefore called deoxy-sphingoid bases (DSBs). The two identified metabolites originate from the conjugation of palmitoyl-CoA with alanine and

glycine instead of serine. This reaction would result in the formation of the two atypical sphingolipids with the lack of the hydroxyl and hydroxymethyl groups at C1 (Fig.24).

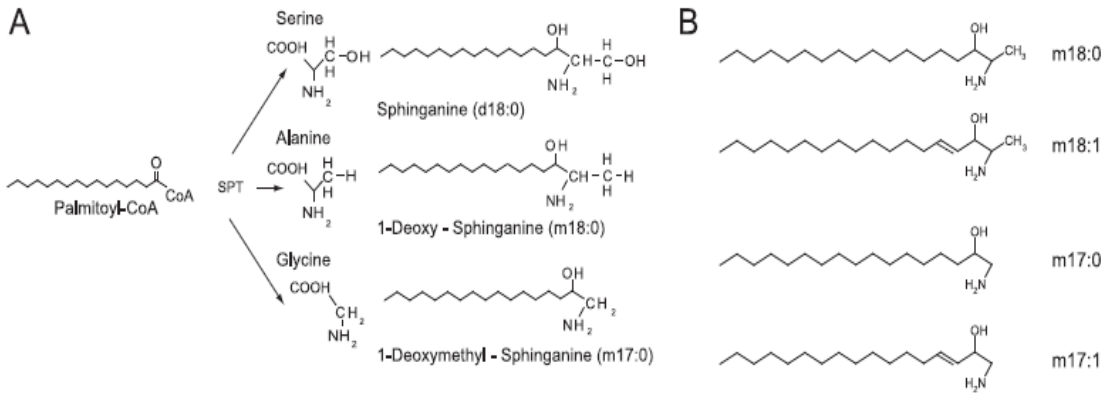

Fig. 24: (A) *Products of the SPT reaction using serine, alanine, or glycine as substrates. The conjugation of palmitoyl-CoA with alanine and glycine leads to the formation of the two DSBs: m18:0 and m17:0.* ***(B)*** *Chemical structure of the DSBs. The numbers of hydroxyls are designated by m (for mono-) and d (for di-) followed by the number of carbons. The second number indicates the double bonds. For example, d18:0 stands for sphinganine, and d18:1 stands for sphingosine. All shown metabolites were also found in the N-acetylated form.*

Indeed, when HEK133W and HEK133Y cells treated with alanine (10 mM) and glycine (10 mM), and the *de novo* synthesis is blocked with FB1, the levels of 1-deoxy-sphinganine and 1-deoxymethyl-sphinganine were increased, respectively, 4-fold and 10-fold suggesting that the HSAN1 mutations induce a shift in the substrate affinity of SPT from serine toward alanine and glycine (Fig.25).

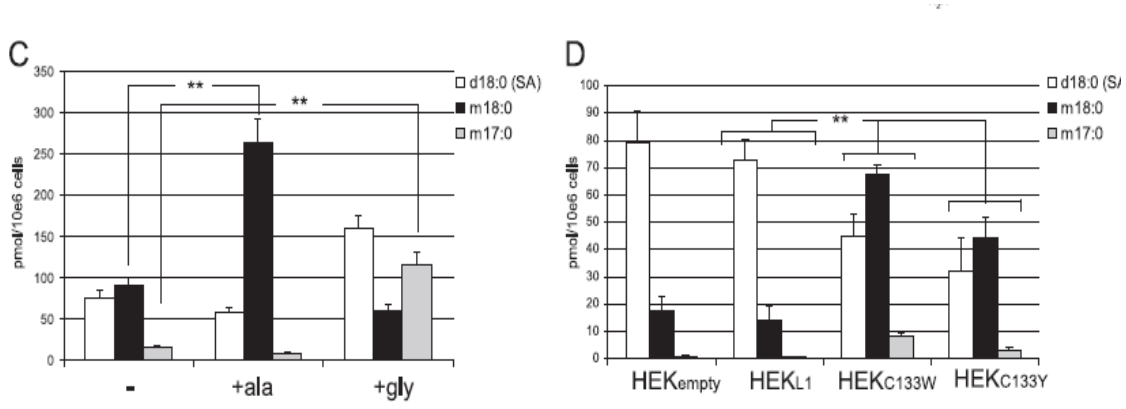

Fig. 25: (C) *Accumulation of m18:0 and m17:0 in HEKC133W cells after supplementing the culture medium with alanine or glycine. HEKC133W cells were cultured using either standard medium (-) or medium that was supplemented with 10mM alanine (-ala) or 10mM glycine (-gly). De novo synthesis was blocked with FB1 for 24 h, and the accumulated lipids were analyzed by LC-MS.* ***(D)*** *Accumulation of DSB in HEK cells expressing mutant forms of SPT. HEKempty, HEKL1, HEKC133W, and HEKC133Y cells were treated with FB1 for 24 h, and the extracted lipids were quantified by LC-MS. Error bars in C and D indicate S.E. p values ≤ 0.01 were labeled with **.*

DSBs are successively metabolized but not in the classical pathway. The lack of the hydroxyl and hydroxymethyl groups inhibit the formation of higher substituted sphingolipids, such as phospho- and glycosphingolipids, but these substrate can't be degraded by the classical pathway because of the inability to format a phosphoester bond at C1. Furthermore, DSBs are substrate for ceramide synthase, *N*-acylated and also desaturated by ceramide desaturase (*DES*), which results in the formation of deoxy-ceramide and deoxy-methyl-ceramide (demonstrated by the elevated levels of deoxy-sfingosine and deoxy-methyl-sphingosine in lipid extraction). Indeed, in the human HSAN 1 plasma higher levels of unsaturated DSBs (than saturated type) has been detected. Furthermore, the highest DSBs levels are correlates with the most severe HSAN1 phenotype while moderately elevated DSBs levels are correlated with moderate HSAN 1 phenotype. Quantitative analyses revealed a dose-dependent effect of DSBs on neuritis growth and also in a significant dose-dependent reduction of neuritis length. Indeed, when DRG (dorsal root ganglia) cultured neurons are added of SA (1 µM), 1-deoxy-sphinganine (1 µM) and 1-deoxy-methylsphinganine (1 µM) it results in a reduction of cells that presents 1 or more neuritis (30% reduction) compared with the control take place suggesting that DSBs disturb neuritis formation. Furthermore, when DSBs are added to SA cultured cell, it results in significant regression of the already formed neuritis. Immune-fluorescence analyses suggest that DSBs change the stability and dynamics of neurofilament formation. Indeed, actin and neurofilament are co-locatizated over the whole length of the neuritis in neurons which are cultured in the presence of SA while the neuritis of neurons that are cultured in the presence of 1-deoxy-sphinganine has a clearly disturbed cytoskeletal structure. The neurofilament straining is significantly shortened and only partly co-localized with the actin, whereas the actin is detected over the whole length of the neuritis suggesting that the pathological mechanism in HSAN1 is the accumulation of these neurotoxic metabolites rather than the reduced *de novo* sphingolipid synthesis[95]

8. Melanoma

Melanoma is the most common and the most aggressive skin cancer originating from neural crest–derived melanocytes, pigment cells present normally in the epidermis and sometimes in the dermis. Melanoma can metastasize to any organ, the brain being a particularly common site. Metastatic melanoma is generally incurable, with survival in patients with visceral metastases generally less than 1 year. This is mainly due to multidrug and radiotherapy resistance by deregulation of apoptotic pathways. Ceramide and sphingosine have been implicated to be lipid signaling molecules in regulation of apoptosis, while sphingosine- 1-phosphate has been reported to be a trigger for signal transduction pathways of cell proliferation[90]**.** Ceramide has a central role in both apoptotic and mitogenic pathways (especially phosphorylated ceramide/sphingosine) and is often generated in response to chemotherapeutics and radiotherapeutics via hydrolysis of sphingomyelin by activated sphingomyelinase (SMase)[91,92]**.** Moreover, an increased cellular capacity for ceramide glycosylation has been identified as a multidrug resistance mechanism. Indeed, multidrug resistant cell types have been reported to display an altered sphingolipid composition, frequently represented by increased level of glucosylceramide[93]**.** Natural products have been proposed as possible treatment for multi-drug resistant melanoma. Myriocin, ISP-1 or thermozymocidin, in addition of the inhibitor activity of the first step of *de novo* sphingolipid biosynthesis pathway, which reduces the intracellular pool of sphingolipid intermediates, also decreases extracellular sphingomyelin, sphingosine-1-phosphate (which has been reported to induce prostate cancer cell migration[94,95] and glycosphingolipids levels[96,97]. Myriocin has been shown to inhibit proliferation of a certain IL-2- dependent mouse cytotoxic T-cell line[98]. Treatment of B16F10 cells (originating from a murine malignant melanoma) with myriocin cause cell numbers decrease and inhibition of cell proliferation by approximately 70% compared to that of controls. The inhibition resulted in both concentration- and time-dependent relation. Furthermore, cell migration when determined by a wound-healing assay result in an inhibition by 69% to 73% compared to those of concurrent controls. Incorporation of [^{3}H] thymidine in B16F10 cells result decreased when cultured with 10 µM myriocin suggest a decreased DNA synthesis of about 50% compared to control. DNA synthesis appears correlated with cell population growth in a time-dependent manner. When analyzed, accumulation of cells in G2 /M occurred after addition of myriocin. The percentage of B16F10 cells, treated with

myriocin, in the G2/M phase appear greatly increased in comparison with control suggesting that myriocin inhibit cell proliferation by G2/M arrest during cell cycle progression. Myriocin-induced inhibition of cell proliferation may occur through both inhibition of cdc25C and activation of p53 and $p21^{waf1\ /\ cip1}$ signalling pathways leading to cell cycle arrest at G2/M phase. Notably, no cell death for apoptosis occurs.

The mechanism myriocin induce cell cycle arrest by, is through regulation of the activity of the protein controlling cell cycle. Cdc2 and cyclin B1 are essential for the regulation of the crossing from G2 to M phases. These proteins are usually inactivated through phosphorylation by Weel's protein-kinase, whereas de-phosphorilation causes activation and cell cycle promotion. The tumor suppressor protein p53 arrest the cell cycle in G2/M phase after DNA damage, hypoxia and expression of mutant oncogenes (Fig.26)[99].

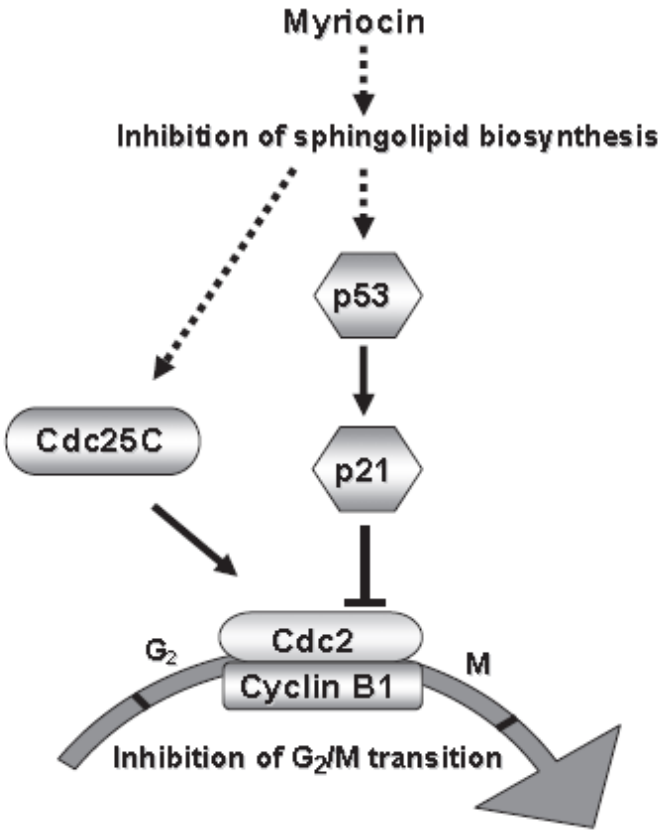

Fig. 26: *Proposed signaling pathways involved in cell cycle arrest induced by myriocin in malignant melanoma cells.*

In B16F10 cells treated with myriocin, the levels of p53 result increased that bring to activation or decrease transcription of several genes involved in its upstream control. Indeed, one of the p53 transcription target cyclin-dependent kinase inhibitor (CIK) $p21^{waf1\ /}$

^{cip1} found overexpressed in B16F10 cells treated with myriocin, binding to and inhibiting activity of the cyclin B1/cdc2 with consequently cell cycle arrest in G2 phase[100].

Chk2 (checkpoint kinase 2) and PLK1 (serine/threonine-protein kinase) can modulate Cdc25 by stimulating the Cdc2/ciclin B1 complex, directly inhibited by Weel's protein kinase[101]**.** The levels of these proteins in B16F10 cells appear to be not altered in comparison with control suggest that the myriocin-induced cell cycle arrest occurr through the p53- p21 signalling pathway[102]. In addition, when treated with caffeine, well known to stimulate several phosphatase leading to de-phosphorilation of p53, the B16F10 cells treated with myriocin revealed a decreased of p53, p-p53 and $p21^{waf1\ /\ cip1}$. However, caffeine did not reverse the effect of myriocin on cell proliferation.

The decreased of ceramide levels and the reduced level of cdc2/ciclin B1 in B16F10 cells was reversed by adding C8-ceramide, suggesting the essential role of endogenous sphingolipids in the tumor growth. Myriocin decrease ERK phosphorylation, well-known to stimulate tumourigenesis, and modulate PKC activity[103]. Furthermore, myriocin decrease the level of gangliosides GD3, highly expressed in malignant melanoma cells and enhances their properties in mice and this could play role in the anti-proliferative activity of myriocin in B16F10 cells[104].

INTRODUCTION TO

EXPERIMENTAL PART

Sphingolipids (SLs) are components of membrane lipid layer ubiquitously distributed in mammalian, bacteria and fungi cells. SLs metabolites modulate different cellular events, such as proliferation, differentiation and apoptosis. Therefore, SLs metabolism modulators may represent powerful tools in biochemical and pharmacological studies. The first step of sphingolipid biosynthesis is represented by the condensation of L-serine and palmitoyl-CoA, catalysed by serine palmitoyltransferase (SPT). Several natural compounds have been found to be powerful SPT inhibitors. However, these substances have structure similarities to the sphingolipid metabolite sphingosine, which modulate several biochemical events in cellular metabolism. Several natural products have been identified as SPT inhibitors even if these compounds are able to interfere in other biochemical pathways. L-cycloserine and β-chloro-L–alanine have been studied as SPT inhibitors in intact cells. Unfortunately these compounds inhibit several PLP-dependent enzymes avoiding a clinical use. Natural compounds as myriocin and viridofungines have been studied as powerful SPT inhibitors. Myriocin inhibits sphingolipids biosynthesis through inhibition of SPT rate and furthermore, Myriocin is a potent immunosuppressant (more than 100 fold than cycloserine according to several studies) which may preclude a long term using in chronic pathologies. However, myriocin has been revealed an important tool which allowes investigation of SPT as new therapeutic target for treatment of atherosclerosis and retinitis pigmentosa (RP). Viridofungines are natural SPT inhibitors less active than myriocin but these derivatives are able to inhibit several enzymes susceptible to tri- and di-carbossilic acids like squalene synthase.[34] Looking at non-natural SPT inhibitors the only data reported are represented by a patent[111] developed by Bolton and colleagues. Neurodegenerative disease treatment represent a huge focus of pharmaceutical research. In the last few years SPT role as innovative target in neurodegenerative disease treatment has been highlighted.

Our research group, have developed different compounds as new SPT inhibitors. Referring to literature compounds of formula **1** (described in the patent[111]) have been evaluated as starting point to advance new SPT inhibitor. Several structural analogues (not present in the patent) have been synthesized. Biological data showed interesting indications of substituent's type and position on the central core. One of the most interesting derivatives obtained is represented by compound **2** which have inhibitory activity in the order of micromolar range. The aim of the present thesis work, was to

evaluated the influence of central core (2-oxo-benzimidazole) in the inhibitor-enzyme interaction. During thesis work have been developed compound of general formula **3**, **4**, **5** and **6** (Fig.27). Such modifications have been mainly directed toward the oxo-benzimidazole core in order to verify electronic and conformational influences of the bicycle nucleus in interaction with enzyme.

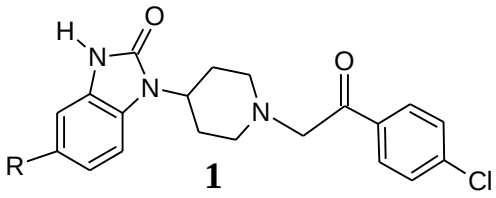

1

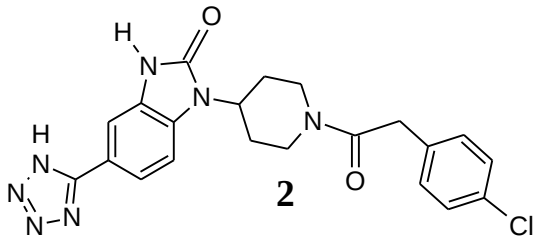

2

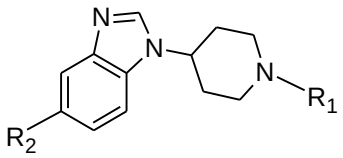

3

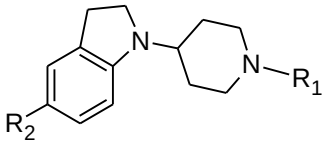

4

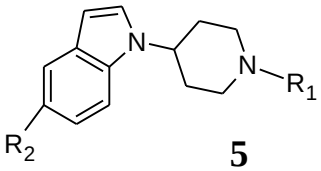

5

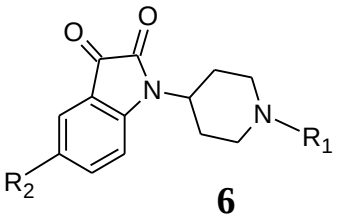

6

Fig. 27

Results and discussion

The derivatives of general formula **3** (Scheme 1) were synthesized starting from 4-chloro-3-nitro-benzonitrile which is subjected to a SN_{Ar} with 4-amino-1-Boc piperidine, leading to **7**. In order to reduce reaction time, the synthetic procedures was developed using a microwave system obtaining very good yields (90 %) which reduced with H_2 and Pd/C to obtain derivative **8** which subsequently was cyclizated in presence of trimethyl ortoformate at 148 °C for 1h to obtain the desired compound **9**. The crude mixture was purified by flash chromatography leading to 60% yield. To improve reaction yield , derivative **8** was cyclizated using a microwave system in presence of trimethyl ortoformate and formic acid at 180°C for 40 minutes. After flash-chromatography purification the desired compound **9** was obtained in good yields (75 %). Then the carbammic group of compound **9** has been hydrolyzed in acidic environment using a trifluoroacetic acid and dichloromethane mixture (65% yields) or using a solution of hydrochloric acid in hydro-alcoholic solution (80% yields) leading to compound **10**. The desired compound was obtained after neutralization of the crude mixture as precipitate. Moreover a synthetic procedure involving direct cyclization of **8** with formic acid to obtain compound **10** has performed. Unfortunately purification of the crude mixture was difficult in relation to compound solubility.

Compound **10** was reacted with *p*-chlorophenylacetyl chloride or 2-bromo-*p*-chloroacetophenone in order to obtain compounds **11a** and **11b** respectively. The derivative **11a** was obtained in good yields (65%) after purification by flash-chromatography. Conversely, the crude product of **11b** was very complex and the desired compound was obtained in very low yields (18%). Unfortunately subsequent modification of the procedure has not improved reaction yields. As described in literature, the cyano-derivatives **11a** and **11b** were converted to compounds **12a** and **12b** after reaction with azido(trimethyl)silane and tetra- N-butylamino fluoride (TBAF) at 130°C for 48h[112]. The final compound **12a** was filtered off after treatment of the crude mixture with a 2M aqueous solution of hydrochloric acid (40% yields) without needs of further purification process. Compound **12b** was subjected to different purification procedures (flash-chromatography, crystallization etc.) without success. Nowadays, procedures to obtain the compound **11b** are in progress.

SCHEME 1

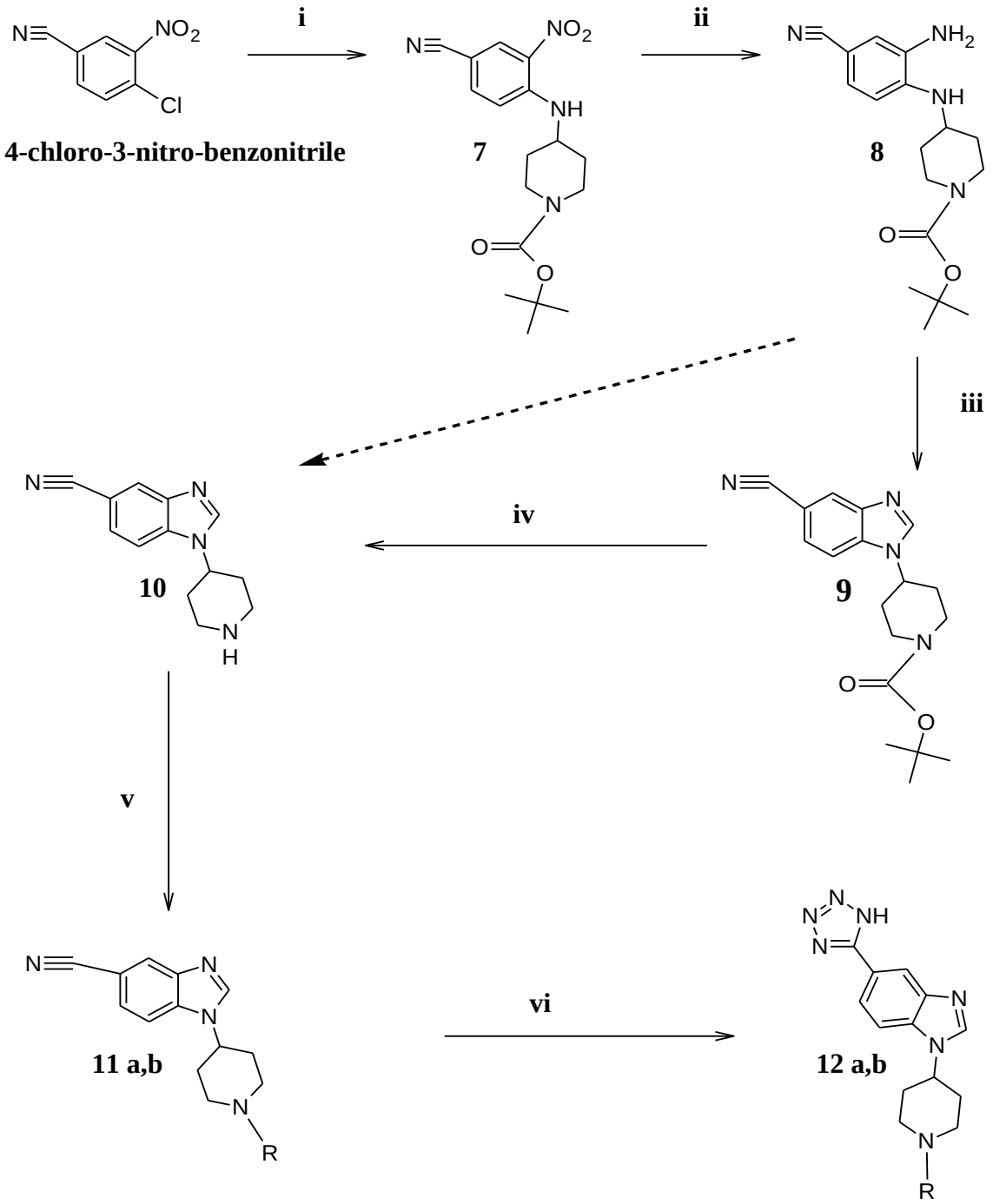

a: R= *p*-chlorophenylacetyl **b**: R= *p*-chlorophenylacyl

Reagents and conditions: (i) DIPEA, DMF, 4-amino-1-Boc-piperidine, microwave, 130°C, 15 min, 5 bar; **(ii)** THF, H_2, EtOH, Pd/C, r.t., 4h; **(iii)** toluene, trimethyl ortoformiate, formic acid, microwave, 180°C, 40 minutes, 9 bar; **(iv)** hydrochloric acid, ethyl acetate; methanol, r.t. 1h; **(v) a:** DMF, THF, triethylamine, *p*-chlororphenylacetyl chloride, r.t. 2h; **b**: DMF, THF, triethylamine, 2-bromo-*p*-chloroacetophenone r.t. 2h; **(vi)** azido(trimethyl)silane, TBAF, N_2, 120°C, 48h.

Different synthetic strategies were evaluated to synthesized compounds of general formula **4**, **5** and **6** and it was identified as building block molecule the indoline derivatives **14.** This molecule is an useful tool to synthesize indole derivatives substituted in position 1 with a piperidine ring whose insertion is diffucult to obtain using other synthetic approach (such as reaction between the indole core and a 4-methylsulfonyloxy-pipertidine derivative)[113]. As well as indole system, the insertion of piperidine group on the isatine core is difficult to perform, whereas direct oxidation of substituted indole lead to isatine derivatives in good yield[114]. On the basis of these observations, a synthetic strategy characterized by the use of **14** as building block has been pursued (Fig. 28).

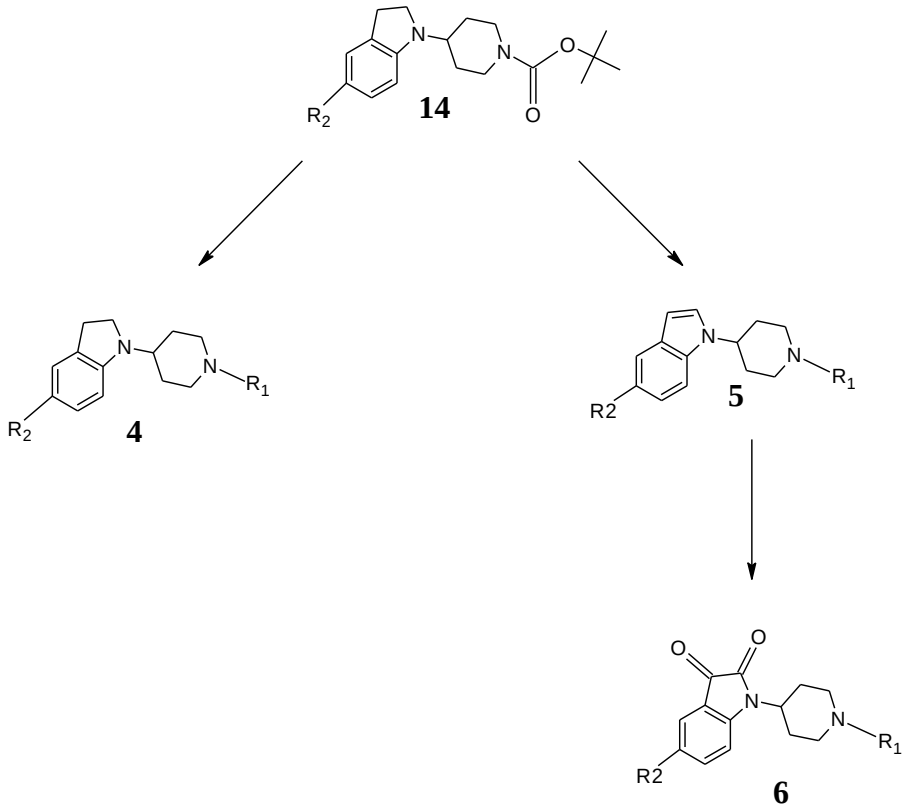

Fig. 28

A commercial available indoline was reacted (Scheme 2) with bromine in dichloromethane at -30°C leading to the 5-bromo-indoline compound **13** (accordingly with literature)[115].

The crude mixture was purified by flash-chromatography (70% yield). Afterwards, a direct reductive amination reaction between the derivative **13** and 1-Boc-4-piperidone has been performed**.** The immine produced was reduced *in situ* by addiction of sodium triacetoxyborohydride. This reductive agent was selected in order to avoid reduction of the ketone and formation of toxic by product (produced by reducing agent such as sodium cyanoborohydride)[116]. The desired compound **14** was obtained in good yields (80%) as a white powder after purification by flash-chromatography. As previously described, the piperidine protective group (Boc) of **14** was hydrolyzed in acidic environment and the pure product was obtained after alcalinization as precipitate which was collected, identified and characterized as **15**. Finally, **15** reacted with *p*-chlorophenylacetyl chloride or 2-bromo-*p*-chloroacetophenone in presence of triethylamine to obtain compound **16a** and **16b** respectively. Purification of crude mixtures showed the same problem noticed for **12a** and **12b**. The derivative **16a** was purified by flash chromatography whereas the derivative **16b** was a complex mixture hardly purified. Procedures to obtain the desired compound **16b** are currently in progress. [The synthetic procedures have revealed that the **b** (p-chloroacetophenyl) substituent makes the compounds difficult to purify and characterize: for this reason synthetic procedure characterized by use of the substituent **a (***p*-chlorophenylacetyl**)** only has been pursued**]**.

Subsequently, accordingly with literature[117] the bromo-derivative **14** was converted to the cyano-derivative **17** avoiding the use of toxic reagents such as sodium cyanide: it was heated in presence of potassium hexacyanoferrate(II) trihydrate, tetrakis(triphenylphosphine)palladium(0), and 1,8-diazabicyclo[5.4.0]undec-7-ene (DBU) in a mixture of *tert*-butanol and water under nitrogen atmosphere to obtain the compound **17** which was purified by flash-chromatography (75% yields) (Scheme 2). The compound **18** was obtained applying the same reaction conditions and purification procedures used to obtain **15**. Compound **18** was subsequently reacted with *p*-chlorophenylacetyl chloride in presence of triethylamine. The crude product was purified by flash-chromatography to yield the desired compound **19a** (60%) whose inhibitory activity was evaluated. Reaction of derivative **19a** with azido(trimethy)silane and TBAF in nitrogen atmosphere led compound **20a** (Scheme 2).

SCHEME 2

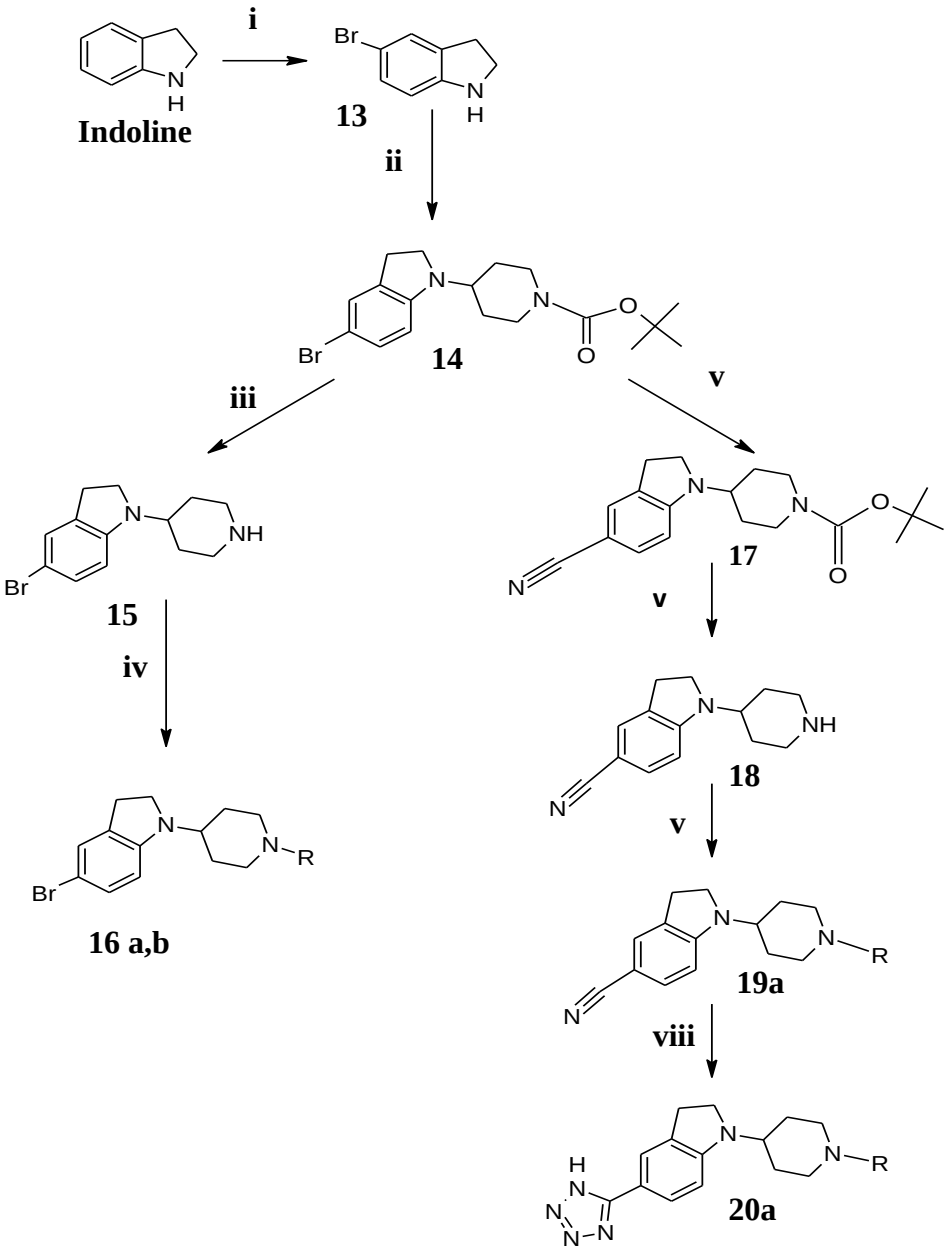

a: R= p-chlorophenylacetyl **b:** R= *p*-chlorophenylacyl

Reagents and conditions: **(i)** dichloromethane, bromine, -30°C, 2h; **(ii)** dichloromethane, 1-Boc-4-piperidone, acetic acid (glacial), sodium triacetoxyboronhydride, 0°C, 15 minutes; r.t. 3h; **(iii)** hydrochloric acid (32%), ethyl acetate, methanol, 4h; **(iv) a**: DMF, THF, p-chlorophenylacetyl chloride, triethylamine, r.t., 3h, **b**: DMF, THF, triethylamine , 2-Bromo-p-chloroacetophenone, r.t., 3h. (**v**) hydrochloric acid (32%), ethyl acetate, methanol, 4h; (**vi**) hydrochloric acid (32%), ethyl acetate, methanol, 4h; (**vii**) DMF, THF, p-chlorophenylacetyl chloride, triethylamine, r.t., 3h; (**viii**) azido(trimethyl)silane, TBAF, 120°C, 48h.

In order to obtain indole derivatives of formula **5** (Scheme 3), compound **14** was oxidized using 2,3-dichloro-5,6-dicyano-1,4-benzoquinone (DDQ) at 0°C for 3 h leading to the compound **21** as described in letterature[118]. The pure product was obtained after purification by flash-chromatography in very good yield (90%). As well as performed for indoline derivatives, indole derivatives substituted with different functional group in position 5 were synthesised. As described previously, **21** was hydrolyzed to **22** and reacted with *p*-chlorophenylacetyl chloride; the crude mixture was purified by flash chromatography leading to compound **23a** (60% yields). Moreover, compound **21** was subjected to the same synthetic *iter* applied to obtain compounds **17** (scheme 2) to obtain the cyano-indole derivatives **24** which was deprotected leading to compound **25** (Scheme 3). Subsequently, applying the same reaction conditions as described previously in scheme 2, starting from compound **25,** compounds **26a** and **27a** were obtained consequently. These compounds were purified by flash-chromatography (**26a**) or precipitation (**27a**).

SCHEME 3

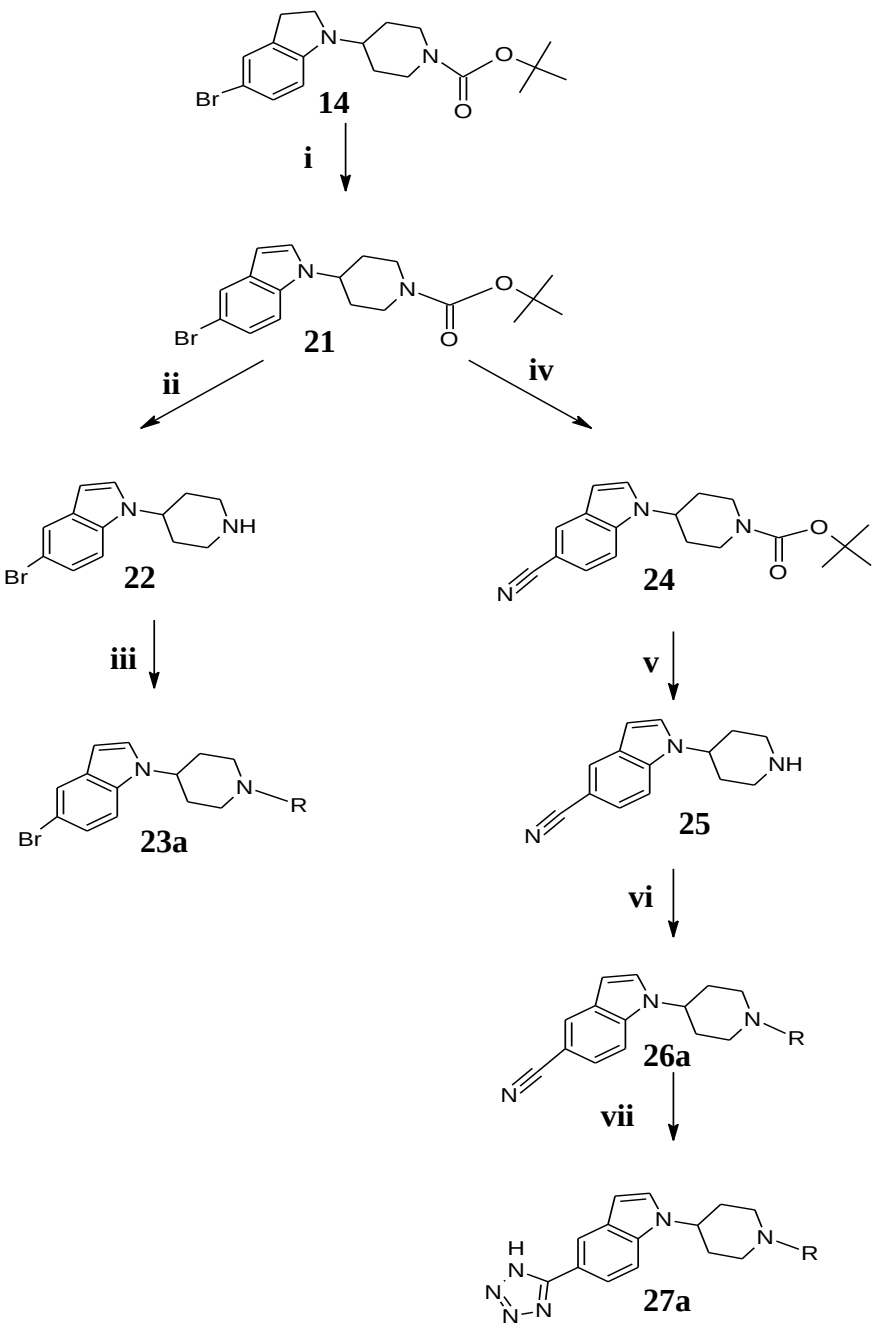

R= *p*-Chlorophenylacetyl

Reagents and conditions : (i) THF, DDQ, 0°C, 3h; **(ii)** ethyl acetate, methanol; hydrochloric acid (32%), r.t., 2h; **(iii)** DMF, THF, triethylamine, *p*-chlorophenylacetyl chloride, r.t., 12h; **(iv)** potassium hexacyanoferrate(II) trihydrate, TPP-Pd; *tert*-butanol/ water, DBU, r.t. 10 min, 85°C, 24h; **(v)** ethyl acetate, methanol; hydrochloric acid 32 %, 30°C, 3h **(vi)** DMF, THF, triethylamine, *p*-chlorophenylacetyl chloride, r.t., 12h; **(vii)** azido(trimethyl)silane, TBAF, 120°C, 48h.

To synthesize the isatine derivatives of general formula **6**, the 5-bromo-indole derivative **21** was oxidized with chromium oxide (VI) at room temperature for 2h (Scheme 4). After neutralization and purification by flash chromatography of the reaction mixture the desired compound **28** was obtained as orange powder (28% yields). The bromo-isatine derivative **28** was heated in presence of potassium hexacyanoferrate(II) trihydrate, tetrakis(triphenylphosphine)palladium(0), and 1,8-diazabicyclo[5.4.0]undec-7-ene (DBU) in a mixture of *tert*-butanol and water under nitrogen atmosphere to obtain the compound **29**. Unfortunately, a complex reaction mixture was obtained not allowing isolation of the desired compound. Purification procedures to obtain the isatine derivative **29,** as precursor for final compounds of general formula **6a** are still under development.

SCHEME 4

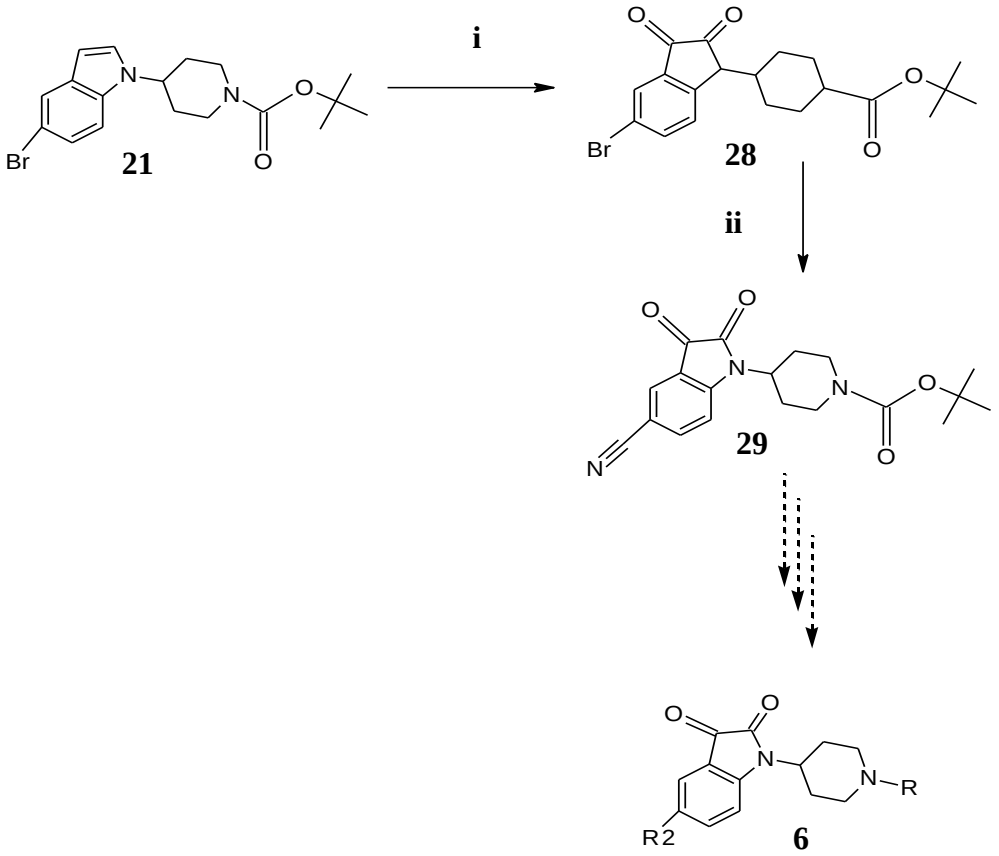

R= *p*-Chlorophenylacetyl

Reagents and conditions : (i) acetone, acetic acid, water, chromium(VI) oxide, r.t., 2h; **(ii)** potassium hexacyanoferrate(II) trihydrate, TPP-Pd; *tert*-butanol/ water, DBU, r.t. 10 minutes; 85°C, 24h.

The inhibitory activity on SPT of the final products was evaluated using a radioactive assay at the research lab of Prof. Ghidoni (Lab Biochem & Mol Biol, San Paolo Medical School, University of Milan). The enzyme source used was a HEK293 cell lysate. Each compound was tested in final concentration of 50 μM (Table 1). The reference compound **2** showed higher inhibitory activity (74% at 50μM) than all the developed compounds.

TABLE 1

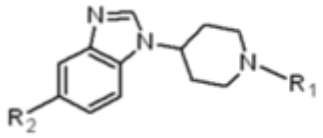

3

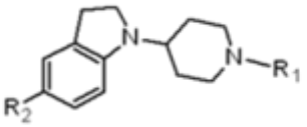

4

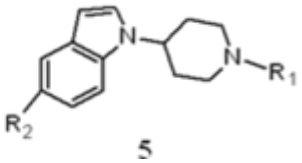

5

Table 1				
Comp.	**R_2**	**R_1**	**Formula**	**% Inhibition**
11a	CN	*p*-chlorophenylacetyl	3	0%
12a	Tetrazole	*p*-chlorophenylacetyl	3	33%
11b	CN	*p*-chloroacetophenyl	3	57%
16a	Br	*p*-chlorophenylacetyl	4	0%
19a	CN	*p*-chlorophenylacetyl	4	1%
20a	Tetrazole	*p*-chlorophenylacetyl	4	31%
23a	Br	*p*-chlorophenylacetyl	5	14,29%*
26a	CN	*p*-chlorophenylacetyl	5	25,92%*
27a	Tetrazole	*p*-chlorophenylacetyl	5	29,04%*

***Preliminary data.**

EQUIPMENT USED

- Melting points were determined on a Kofler hot stage apparatus and are uncorrected.

- ^{1}H NMR and ^{13}C NMR spectra were recorded with a Bruker AC-200 spectrometer in δ unit from TMS as an internal standard.

- Analytical TLC was carried out on Merck 0.2 mm precoated silica-gel glass plates (60 F-254) and location of spots was detected by illumination with a UV lamp.

- Microwave used was a Biotage Initiator EXP EU, 355301, 11443-11X, 400W, 2450 MHz.

EXPERIMENTAL PART

tert-Butyl 4-(2-nitro-4-cyanophenylamino)-piperidine-1-carboxylate (7)

In a microwave vial containing 3.5 mL of N,N-diisopropylaethylamine, (DIPEA, d=0.742) and 4 mL of dimethylformamide (DMF), 1.826 g (10 mmol) of 4-chloro-3-nitrobenzonitrile were dissolved. Afterwards, 2.4 g of 4-amino-1-Boc-piperidine were added and the mixture was placed in microwave device. Reaction conditions: 15 minutes; 130°C; 5 bar. After cooling, the reaction mixture was added of 50 mL of ethyl acetate and 10 mL of tetrahydrofuran (THF). The organic layer was washed with 0.5 M solution of hydrochloric acid (2x40 mL) and brine in a separatory funnel. The organic layer was dried over magnesium sulfate, filtrated and evaporated *in vacuo* leading to the desired compound as a yellow powder.

The titled compound was obtained as a pure product crystallizing achieved using toluene.

Yield: 90%

M.W.: 346.38; $C_{22}H_{22}O_4N_4$

Mp: 143-145°C

^{1}H NMR (DMSO, 200 MHz): δ 8.52 (s, 1H, Ar), 8.25-8.21 (m. 1H, Ar), 7.86-7.82 (m, 1H, Ar), 7.35-7.30 (m, 1H), 3.95-3.88 (m, 2H), 3.1-2.8 (m, 2H), 1.96-1.85 (m, 2H), 1.55-1.48 (m, 9H, Boc)

tert-Butyl 4-(2-amino-4-cyanophenylamino)-1-piperidinecarboxylate (8)

An amount of 1.21 g (3.49 mmol) of *tert*-butyl 4-(2-nitro-4-cyanophenylamino)-1-piperidinecarboxylate **(7)** was solubilized in 120 mL of a solution of THF (5%) and absolute ethanol (95%). The solution obtained was added of Pd/C, placed under hydrogen and stirred at room temperature for 4h. Afterwards, the solution was filtrated on a silica pad and washed with ethyl acetate (100 mL). The organic phase was eliminated *in vacuum* leading to a white powder.

The title compound was obtained crystallized using isopropanol.

Yield: 90%

M.W.: 316.4; $C_{24}H_{24}0_2N_4$

Mp: 160°-162° C

^{1}H NMR ($CDCl_3$, 200 MHz): 7.17-7.13 (d, 1H, Ar), 6.96 (s, 1H, Ar), 6.63-6.58 (m, 1H, Ar), 4.106-3.92 (m, 4H), 3.47-3.29 (m, 2H), 3.02-2.96 (m, 2H), 2.08- 2.02 (m, 2H), 1.6-1.26 (m, 9H, Boc).

***tert*-Butyl 4-(5-cyano-1H-benzimidazol-1-yl)piperidine-1-carboxylate (9)**

Method A

An amount of 0.632 g (2 mmol) of *tert*-butyl 4-(2-amino-4-cyanophenylamino)-1-piperidinecarboxylate (**8**) was solubilized in 5 mL of trimethyl ortoformiate (45 mmol, d=0.97 g/mL). The solution was heated at 148°C (reflux) for 1h. Afterwards, the solution was cooled and the solvent evaporated *in vacuum*. The crude mixture was purified by flash chromatography (eluent ethyl acetate). The combined fractions were evaporated leading to the pure product as a white powder.

Yield A: 60 %

Method B

A solution of 0.88 g (2.78 mmol) of *tert*-butyl 4-[(2-amino-4-cyanophenyl)amino]piperidine-1-carboxylate **(8)** in toluene (5 mL) was added of 3.7 mL (27.8 mmol, d=0.97 g/mL) of trimethyl ortoformiate and 10 µL (0.265 mmol, d=1.22 g/mL) of formic acid. The solution was placed in microwave equipment (180°C; 40 minutes and 9 bar). After cooling, the reaction was added of water and extracted with toluene. The organic layer was dried over magnesium sulfate and evaporated *in vacuum*. The crude mixture was purified by flash chromatography (ethyl acetate and *n*–hexane; 5:1). The combined fractions were evaporated leading to the pure product as a white powder.

Yield B: 75 %

M.W.: 326.39; $C_{18}H_{22}O_2N_4$

Mp: 115-116°C

^{1}H-NMR (200 MHz $CDCl_3$): δ 8.15 (s, 1H, N=CH-N); δ 8.11 (s, 1H, Ar); δ 7.55 (dd, 2H, Ar), δ 4.39 (m, 4H), δ 3.0-2.95 (t, 2H), δ 2.95 (t, 2H), δ 1.50 (s, 9H, Boc).

1-(piperidin-4-yl)-1*H*-benzimidazole-5-carbonitrile (10)

Method A:

An amount of 0.51 g (1.56 mmol) of *tert*-butyl 4-(5-cyano-1*H*-benzimidazol-1-yl)piperidine-1-carboxylate **(9)** was solubilized in 25 mL of ethyl acetate and methanol mixture (1:1). The solution was added, of 6 mL of a 32% solution of hydrochloric acid. After 1h the solution was concentrated *in vacuum* and the residue was added of a saturated solution of sodium bicarbonate until pH=8. The obtained solution was extracted with chloroform and the organic layer was dried over magnesium sulfate, filtrated and solvent evaporated in vacuum. The title compound was collected as a white powder.

Yield A: 65 %

Method B:

0.326 g (1 mmol) of *tert*-butyl 4-(5-cyano-1*H*-benzimidazol-1-yl)-piperidine-1-carboxylate **(9)** was solubilized in 10 mL of dichloromethane. After that, 0.8 mL of trifluoroacetic acid was added and the reaction stirred at room temperature. After 2h the solution was concentrated in vacuum, and the residue added a saturated solution of sodium bicarbonate until pH=8. The obtained solution was extracted with chloroform and the organic layer was dried over magnesium sulfate, filtrated and solvent eliminated in vacuum. The title compound was collected as a white powder after dried over in vacuum overnight.

Yield B: 80 %

M.W.: 226. 28; $C_{13}H_{14}N_4$

M.p.: 170°-172°C

^{1}H-NMR: DMSO δ 8.732 (s, 2H, NHH, br), 8.55 (s, 1H, N=CH-N) 7.95(d, 1H, Ar), δ 7.912 (d, 1H, Ar), 4.80 (m, 1H, N-CHCC), 3.52 (m, 2H), 3.18 (m, 2H), δ 2.49 (m, 2H), 2.23 (m, 2H);

^{13}C-NMR: DMSO δ 169.3 (C=O), 143.7 (C), 142.7(CH), 135.8 (C), 133.3 (C), 133.2 (C), 130.2 (CH_2), 129.3 (CH_2), 126.5 (CH), 126.1 (CH), 119.7 (C), 111.1 (CN), 106.3 (C), 54.3 (CH_2), 45.5 (CH), 41.5 (CH), 40.6 (CH_2), 32.7 (CH), 31.9 (CH).

1-(1-(2-(*p*-chlorophenyl)acetyl)piperidin-4-yl)-1H-benzimidazole-5-carbonitrile (11a)

An amount of 0.23 g (1.0 mmol) of 1-(piperidin-4-yl)-1*H*-benzimidazole-5-carbonitrile **(10)** was solubilized in 2 mL of DMF and 4 mL of THF. The mixture was stirred at room temperature and added of 280 μL (2 mmol, d=0.726 g/mL) of triethylamine and 176 μL (1.2 mmol, d=1.292 g/mL) of 4'-chlorophenilacetyl chloride. After 2h the mixture was concentrated *in vacuum* and cold water was added to the residue. The crude product was extracted with chloroform which was dried over magnesium sulfate and concentrated *in vacuum*. The residue (302 mg) was purified using a BUCHI Sepacore chromatography (10:0.05 ethyl acetate/acetonitrile). The combined fractions were evaporated leading to the pure product as a white powder.

Yield: 65 %

M.W.: 377.87; $C_{21}H_{19}N_3Cl$

M.P.: 177-179 °C

^{1}H-NMR (200 MHz, $CDCl_3$)**:** δ 8.15 (s, 1H, N=CH-N), δ 8.03 (s, 1H, Ar), δ 7.58-7.54 (d, 1H, Ar), δ 7.43-7.21 (m, 7H, Ar), 4.98 (d, 1H, N-CHCC), 4.43-4.37 (m, 1H), 4.14-4.07 (m, 1H), 3.78 (s, 2H), 3.51-3.44 (m, 1H), 3.31-3.18 (m, 1H), 2.85-2.72 (m, 1H), 2.19-1.71 (m, 9H), 1.25-1.18 (m, 2H).

1-{1-[(*p*-Chlorobenzoyl)methyl]piperidin-4-yl}-1H-benzimidazole-5-carbonitrile (11b)

0.230 g (1.0 mmol) of 1-(piperidin-4-yl)-1*H*-benzimidazole-5-carbonitrile **(10)** were dissolved in 2 mL of DMF. The obtained solution was added of 280 μL (2 mmol, d=0.726 g/mL) of triethylamine and 2 mL of a solution of 2-bromo-*p*-chloroacetophenone (0.25 mg) in THF and stirred at room temperature. After 2h the reaction mixture was concentrated *in vacuum*. The residue was added of cold water and extracted with dichloromethane. The solvent was removed *in vacuum* and the crude mixture was dissolved in methanol, adsorbed on silica gel and purified in flash chromatography (ethyl acetate/*n*-hexane 1:7). The combined fractions were evaporated leading to the pure product as a white powder.

Yield: 18 %

M.W.: 378.85; $C_{21}H_{19}ON_4Cl$

M.P.: 157°-159° (crystalized in isopropanol and obtained)

^{1}H NMR (200 MHz $CDCl_3$): δ 8.16 (s. 1H, Ar), 7.99-7.90 (m, 1H, Ar), 7.55-7.26 (m, 5H, Ar), 4.67-4.66 (m, 1H), 3.91 (s, 2H, CH_2), 3.25-3.19 (m, 2H), 2.52-2.05 (m, 3H).

2-(*p*-chlorophenyl)-1-{4-[5-(1*H*-tetrazol-5-yl)-1*H*-benzimidazol-1-yl]piperidin-1-yl}ethanone (12a)

In a screw cap vial, 0.151 g (0.4 mmol) 1-(1-(2-(*p*-chlorophenyl)acetyl)piperidin-4-yl)-1H-benzimidazole-5-carbonitrile **(11a)** were added and stirred under nitrogen atmosphere. Then 110 μL (0.4 mmol, d=0.868 g/mL) of azido(trimethyl)silane and 200 μL (0.2 mmol) of tetra-n-butylammonium floride (TBAF) in THF. Then, the mixture was heated at 120°C for 48h. The crude mixture (brown solid) was cooled at room temperature and washed with a 2M aqueous solution of hydrochloric acid (3 X 5 mL) and ice leading to a yellow precipitate which was filtered and washed with water. The titled compound was crystallized using acetonitrile leading to a yellow powder.

Yield: 40 %

M.W.: 421.89; $C_{21}H_{20}ON_7Cl$

Mp: 225°-227° C

^{1}H-NMR: DMSO δ 9.20 (s, 1H, N=CH), 8.50 (s, 1H, Ar), 8.16-8.15 (m, 2H, Ar), 7.40-7.30 (m, 4H, Ar), 4.90-4.50 (m, 1H, N-CH), 4.20-4.10 (m, 1H), 3.90-3.80 (s, 2H, CH_2), 3.40-3.10 (m, 2H) 2.79-2.73 (m, 2H), 2.13-1.94 (m, 4H).

1-(*p*-chlorophenyl)-2-{4-[5-(1*H*-tetrazol-5-yl)-1*H*-benzimidazol-1-yl]piperidin-1-yl}ethanone (12b)

In a screw cap vial, 0.10 g (0.26 mmol) of 1-{1-[2-(*p*-chlorophenyl)-2-oxoethyl]piperidin-4-yl}-1H-benzimidazole-5-carbonitrile **(11b)** were added of 70 μL of azido(trimethyl)silane (0.52 mmol, d=0.868 g/mL) and 130 μL (0.13 mmol) of tetrabutylamino floride (TBAF) in THF and stirred under nitrogen atmosphere. The mixture was heated at 120°C for 48h. Then the crude mixture (brown solid) was cooled at room temperature and washed with a 2M aqueous solution of hydrochloric acid (3 X 5 mL) leading to a yellow powder. The solid product was filtered and washed with water.

The title compound was hardly to purify.

5-Bromoindoline (13)

1.9 mL (16.8 mmol, d=1.063 g/ml) of indoline were solubilized in 120 mL of dichloromethane and cooled at -30 °C. 40 mL (16.8 mmol, d=3.119 g/ml) of a bromine solution in dichloromethane were added dropwise in 30 min. The reaction was stirred for further 2 h at -30°C. Then a solution of 0.1 N sodium thiosulfate (2x40 mL) was added in order to quench the reaction. The organic phase was dried over magnesium sulfate, filtered and evaporated *in vacuum*. The crude mixture was purified by flash chromatography (5:1; *n*-hexane/ethyl acetate). The combined fractions were evaporated *in vacuum* leading to the pure product as a yellow powder.

Yield: 70%

M.W.: 198.06; C_8H_8NBr

M.P.: 39°-40°C

^{1}H NMR (200 MHz DMSO): δ 7.12 (s, 1H, Ar), 7.03 (d, 1H, Ar), 6.99 (d, 1H, Ar), 6.44-6.39 (s, br, 1H, NH), 3.64(t, 2H, CH_2), 3.14(t, 2H, CH_2);

^{1}H NMR (200 MHz $CDCl_3$): δ 7.21 (s, 1H, Ar), 7.09 (dd, 1H, Ar), 6.50(d, 1H, Ar), 3.57 (t, 3H, CH_2, NH), 3.02 (t, 2H, CH_2);

^{13}C NMR (200 MHz DMSO): δ 151.20 (C), 131.12 (C), 128.66 (CH), 126.22 (CH), 109.05 (CH), 106.50 (C), 46.03 (CH_2), 28.49(CH_2).

tert-Butyl 4-(5-bromo-indolin-1-yl)piperidine-1-carboxylate (14)

An amount of 1.72 g (8.9 mmol) of 5-bromoindoline **(13)** were dissolved in 20 mL of dichloromethane and cooled at 0°C under stirring. Then 1.95 g (9.79 mmol, 1.1 eq) of 1-Boc-4-piperidone, 1.3 mL of glacial acetic acid and 2.83 g (13.35 mmol, 1.5 eq) of sodium triacetoxy borohydride were added. After 15 min the reaction was kept at room temperature and stirred for further 3h. Then the reaction was stopped by addiction of 10 mL of saturated solution of sodium bicarbonate. After the separation from the organic phase, the aqueous layer was extracted with dichloromethane. The organic phases were collected, dried over magnesium sulfate and the solvent was evaporated *in vacuum*. The crude mixture was purified by flash chromatography (5:1, *n*-hexane/ethyl acetate). The combined fractions were evaporated leading to the pure product as a white powder.

Yield: 80%

M.W.: 381; $C_{18}H_{25}O_2N_2$

M.P.: 91°-93 °C

^{1}H NMR (200 MHz $CDCl_3$): δ 7.14 (s, 1H, Ar), 7.11 (d, 1H, Ar), 6.28 (d, 1H, Ar), 4.27-4.22 (m, 1H, CH), 3.36 (tr, 2H, CH), 2.97-2.76 (m, 4H, CH), 1.79-1.74 (m, 3H, CH), 1.64-1.48 (s, 12H, CH_3);

^{1}H NMR (200 MHz DMSO): δ 7.11-7.07(m, 2H, Ar), 6.44-6.40 (d, 1H, Ar), 4.06-3.99 (m, 1H, CH), 3.60-3.33 (m, 1H, CH), 2.89-2.81 (m, 4H, CH), 1.65-1.60(m, 3H, CH), 1.47-1.22 (m, 13H, CH);

5-Bromo-1-(piperidin-4-yl)-indoline (15)

A mixture of 1.143 g (3 mmol) of *tert*-butyl 4-(5-bromo-indolin-1-yl)piperidine-1-carboxylate **(14)** were solubilized in 8 mL of ethyl acetate/methanol (1:1) and 2 mL of hydrochloric acid 32 % and stirred at room temperature. After 4 h a saturated solution of sodium bicarbonate (until pH=8) was added obtaining a precipitate. The solid was filtered *in vacuum* and dryed overnight. The titled compound was collected as white powder.

Yield: 90%

M.W.: 280.188; $C_{13}H_{17}N_2Br$

M.P.: 180-182°C

^{1}H NMR (200 MHz, DMSO): δ 8.97 (br, NH), 7.14(s, 1H, Ar), 7.10 (dd, 1H, Ar), 6.49 (dd, 1H, Ar), 3.70 (m, 1H), 3.35-3.28(m, 6H), 2.93-2.85 (m, 4H), 1.86-1.79 (m, 2H).

^{13}C NMR (200 MHz DMSO): δ 149.06 (C), 132.04 (C), 128.77 (CH), 126.40 (CH), 107.83 (CH), 106.90 (C), 49.02 (CH_2), 45.83 (CH), 42.26 (CH_2), 26.85 (CH_2), 23.49 (CH_2).

1-[4-(5-bromo-indolin-1-yl)piperidin-1-yl]-2-(*p*-chlorophenyl)ethanone(16a)

0.28 g (1.0 mmol) of 5-bromo-1-(piperidin-4-yl)-indoline **(15)** were dissolved in 2 mL of DMF and 4 mL of THF and stirred at room temperature. 276 µL (2 mmol, d=0.726 g/mL) of triethylamine and 176 µL (1.2 mmol) of *p*-chlorophenylacetyl chloride were added. After 3 h the solution was concentrated *in vacuum* and cold water was added. The crude mixture was extracted with dichloromethane, dried over magnesium sulfate, filtered and concentrated. The brown semi-solid obtained was purified by flash chromatography (,ethyl acetate/*n*-hexane; 7:2). The combined fractions were evaporated leading to the pure product as a yellow light powder.

Yield: 55 %

M.W.: 433.756; $C_{20}H_{21}ON_2BrCl$

M.P.: 143°-145°C

^{1}H NMR (200 MHz $CDCl_3$): δ 7.29-7.14 (m, 7H, Ar), 4.83-4.76 (m, 1H), 3.98-3.92 (m, 1H), 3.73 (s, 2H, CH_2), 3.50-2.92 (m, 5H), 2.67.2.61 (m, 1H), 1.86-1.54 (m, 4H).

2-[4-(5-bromo-indolin-1-yl)piperidin-1-yl]-1-(*p*-chlorophenyl)ethanone (16b)

An amount of 0.28 g (1.0 mmol) of 5-bromo-1-(piperidin-4-yl)-indoline (**15**) was solubilized in acetonitrile (10 mL). The solution was added of 280 µL (2 mmol, d=0.727 g/mL) of triethylamine and 2 mL of a solution of 2-bromo-*p*-chloroacetophenone (0.467 mg) in THF and stirred at 75 °C (reflux). The mixture was put to react overnight. Then the reaction mixture was added of cold water and extracted with dichloromethane. The solvent was removed *in vacuum*. The crude product was hard to purify.

tert-Butyl 4-(5-cyano-indolin-1-yl)piperidine-1-carboxylate (17)

A vial was charged with 1.144 g (3 mmol) of *tert*-butyl 4-(5-bromo-indolin-1-yl)piperidine-1-carboxylate **(8)**, 0.507 g (1.2 mmol) of potassium ferrocyanide trihydrate and 86 mg (0.075 mmol) of tetrakis(triphenylphosphyne)palladium(0). The vial was capped, evacuated and backfilled with nitrogen. Subsequently, under nitrogen, 9 mL of a solution of *tert*-butanol/ water (1:1) and 110 µL (0.75 mmol, d=1.018 g/mL) of 1,5-Diazabiciclo[5.4.0]undec-5-ene (DBU) were added. The vial was stirred 10 min at room temperature and then at 85°C (in pre-heated oil bath) for 24 h. The reaction mixture was filtered and the cake was rinsed with 20 mL of methanol and 20 mL of dichloromethane. The organic solution was dried over magnesium sulfate, filtered and evaporated *in vacuum*. The crude product obtained was solubilized in methanol, adsorbed on silica gel and purified by flash chromatography (ethyl acetate). The combined fractions were evaporated leading to the pure product as a white powder.

Yield: 85%

M.W.: 327.43; $C_{18}H_{25}O_2N_3$

M.P.: 130-132 °C

^{1}H NMR (200 MHz, DMSO): δ 7.38 (d, 1H, Ar), 7.27 (s, 1H, Ar), 6.54 (d, 1H, Ar), 4.06-3.99 (m, 2H), 3.69-3.50 (m, 1H), 3.46-3.33 (m, 2H), 2.95-2.80 (m, 4H), 1.661-1.38 (m, 12H,).

^{13}C NMR (200 MHz, DMSO): δ 153.42 (C=O), 153.07 (C), 132.53 (CH), 129.89 (CH), 126.403 (CH), 120.14 (C), 105.09 (CH_2), 95.61 (CH), 78.09 (CH_2), 50.93 (CH_2), 45.43 (CH_2), 27.49 (CH_3), 27.06 (CH_2), 25.09 (CH_2).

4-(5-cyano-indolin-1-yl)piperidine (18)

An amount of 0.9 g (2.75 mmol) of *tert*-butyl 4-(5-cyano-indolin-1-yl)piperidine-1-carboxylate **(17)** was dissolved in 11 mL of ethyl acetate-methanol mixture (1:1) and added of 3 mL of hydrochloric acid 32 % for 2 h. Once the reaction was completed (TLC monitoring)ba saturated solution of sodium bicarbonate was added in order to reach pH=8. After vacuum filtration and drying over overnight, the title compound was collected as a white powder.

Yield: 80%

M.W.:227.3; $C_{14}H_{17}N_3$

M.P.:143-145°C

^{1}H NMR (200 MHz, DMSO): δ 8.94 (br, NH), 7.39-7.35 (d, 1H, Ar), 7.27 (s, 1H, Ar), 6.53-6.48 (d, 1H, Ar), 3.54-3.45 (m, 3H), 3.02-2.88 (m, 5H), 1.57-1.45 (m, 5H).

1-{1-[2-(*p*-chlorophenyl) acetyl] piperidin-4-yl}-indolin-5-carbonitrile (19a)

0.227 g of 4-(5-cyano-indolin-1-yl)piperidine **(18)** (1.0 mmol) are dissolved in 1 mL of DMF and 4 mL of THF,.280 µL of triethylamine (2 mmol, d=0.726 g/mL) and 176 µL (1.2 mmol, d =1.292 g/mL) of *p*-chlorophenylacetyl chloride were. The reaction was stirred at room temperature overnight. The mixture was concentrated *in vacuum* and added of cold water. The crude mixture was washed with water (3x 10 mL) and extracted with dichloromethane. The organic layer was dried over magnesium sulfate and filtered. The solvent was removed *under vacuum*. The crude product was purified by flash chromatography (ethyl acetate). The combined fractions were evaporated leading to the pure product as a yellow powder.

Yield: 40%

M.W.: 379.86; $C_{22}H_{22}ON_3Cl$

M.P.: 163-165 °C

^{1}H NMR (200 MHz $CDCl_3$): δ 7.34-7.18 (m, 6H, Ar), 6.32-6.28 (d, 1H, Ar), 4.86-4.79 (m, 1H), 4.01-3.94 (m, 1H), 3.73 (s, 2H), 3.65-3.37 (m, 3H), 3.14-2.89 (m, 3H), 2.69-2.56 (m, 1H), 1.79-1.58 (m, 3H).

^{13}C NMR (200 MHz $CDCl_3$): δ 169.10 (C=O), 153.86(C), 133.6 (CH), 133.03 (C), 130.68 (CH), 130.24 (CH_2), 129.09 (CH_2), 127.82 (CH), 121.01 (C-CN), 105.68 (CH_2), 98.65 (C), 52.89 (CH_2), 46.85 (CH_2), 45.81 (CH), 41.79 (CH), 28.49 (CH), 28.13 (CH), 27.5 (CH).

2-(*p*-chlorophenyl)-1-{4-[5-(1*H*-tetrazol-5-yl)-1*H*-indolin -1-yl]piperidin-1-yl}ethanone (20a)

A screw cap vial was filled with nitrogen and charged with 0.15 g (0.39 mmol) of 1-{1-[2-(*p*-chlorophenyl) acetyl] piperidin-4-yl}-indolin-5-carbonitrile **(19)**, 104 µL of azido(trimethyl)silane (0.4 mmol, d=0.868 g/mL) and 200 µL (0.195 mmol) of 1M TBAF solution in THF. The vial was capped and heated at 120°C for 48 h. Afterwards the crude mixture (brown semisolid) was cooled at room temperature and washed with a 2M solution of hydrochloric acid (3 X 5 mL) to give a yellow powder. The solid product was filtrated *in vacuum* and washed with water and purified by flash chromatography (ethyl acetate/acetonitrile; 10:1). The combined fractions were evaporated leading to the pure product as a yellow powder.

Yield: 20%

M.W.: 424.91; $C_{22}H_{23}ON_6Cl$

M.P.: 208-210 °C

^{1}H NMR (200 MHz, DMSO): δ 8.26 (s, 1H, Ar), 7.80-7.76 (m, 1H, Ar), 7.62-7.60 (d, 1H, Ar), 7.41-7.26 (m, 4H, Ar), 6.65-6.63 (d, 1H), 4.74-4.57 (m, 1H), 4.16-4.00 (m, 1 H), 3.80-3.75 (m, 2H, OC-CH_2-Ar), 3.32-3.18 (m, 2H), 2.49-1.82 (m, 6H), 1.22-1.13 (m, 3H).

^{13}C NMR (200 MHz, DMSO): δ 211.14 (C), 167.86 (C=O), 134.36 (C), 131.30 (C), 131.16 (C), 131.05 (C), 130.32 (CH_2), 127.50 (CH_2), 126.24 (C), 119.25 (CH), 114.50 (C), 110.20 (CH), 101.62 (CH), 78.50 (C), 66.95 (CH), 52.88 (C), 52.10 (CH).

tert-Butyl 4-(5-bromo-1*H*-indol-1-yl)piperidine-1-carboxylate (21)

tert-Butyl-4-(5-bromo-indolin-1-yl)piperidine-1-carboxylate **(14)** (0.381 g,1.0 mmol) was dissolved in 4 mL of THF. Afterwards, 3mL of a solution of 2,3-dichloro-5,6-dicyano-1,4-benzoquinone (DDQ) (0.27 g, 1.2 mmol) in THF was added dropwise and the solution was stirred at 0°C for 3 h. The reaction mixture was diluted with ethyl acetate (40mL) and was washed with sodium bicarbonate saturated solution (2x20mL) and brine (20mL). The organic layer was dried over magnesium sulfate and the solvent was evaporated *in vacuum*. The crude product was purified by flash chromatography (petroleum ether/ethyl acetate, 5:1). The combined fractions were evaporated leading to the pure product as a white powder.

Yield: 90%

M.W.: 379.31; $C_{18}H_{23}O_2N_2Br$

M.P.: 91-93 °C

^{1}H NMR (200 MHz, DMSO): δ 7.72-7.71 (d, 1H, Ar), 7.58-7.54 (m, 2H, Ar, CH=C), 7.25-7.20 (dd, 1H, Ar), 6.44-6.43 (d, 1H, C=CH), 4.58-4.57 (m, 1H, N-CH), 4.14-4.07 (m, 2H, CH_2), 3.33-2.95 (m, 2H, CH_2), 1.89-1.76 (m, 4H), 1.42 (s, 9H, Boc).

^{13}C NMR (200 MHz, DMSO): δ 153.11 (C=O), 133.34 (C), 129.12 (C), 126.00 (CH), 122.65 (CH), 121.94 (CH), 111.12 (CH), 110.99 (C), 100.16 (CH), 78.24 (CH), 51.86 (CH_2), 31.34 (CH_2), 27.55 (CH_3).

4-(5-bromo-1*H*-indol-1-yl)piperidine (22)

An amount of 0.38 g (1.0 mmol) of tert-Butyl 4-(5-bromo-1*H*-indol-1-yl)piperidine-1-carboxylate **(21)** was solubilized in 5 mL of ethyl acetate and methanol mixture (1:3) and added of 0.5 mL of hydrochloric acid (32 %) and stirred at 30°C. After 3 h, the solution was concentrated *in vacuum* and a saturated solution of sodium bicarbonate was added until pH=8 leading to formation of a precipitate. After vacuum filtration and drying over vacuum overnight, the title compound was collected as a white powder.

Yield: 80%

M.W.: 279.05: $C_{13}H_{15}N_2Br$

M.P.:139-141 °C

^{1}H NMR (200 MHz, DMSO): δ 7.71 (s, 1H, Ar), 7.68-7.44 (m, 2H, Ar, CH=C), 7.24-7.202(m, 1H, Ar), 6.45-6.45 (s, 1H, C=CH), 4.55-4.52 (m, 1H, N-CH), 3.198 (m, 2H), 2.87-2.85 (m, 2H), 1.96-1.76 (m, 6H)

1-[4-(5-bromo-1*H*-indol-1-yl)piperidin-1-yl]-2-(*p*-chlorophenyl)ethanone (23a)

4-(5-bromo-1*H*-indol-1-yl)piperidine (**22**) (0.09 g, 0.3 mmol) was dissolved in 5 ml of a DMF and THF mixture(3:2). The solution obtained, was added of 84 µL (0.6 mmol, d=0.726 g/mL) of triethylamine and 53 µL (0.39 mmol, d=1.292 g/mL) of *p*-chlorophenylacetyl chloride. The mixture was stirred at room temperature overnight. The solution was concentrated *in vacuum*, and cold water was added. The crude product was extracted in chloroform dried over magnesium sulfate and the solvent was removed *in vacuum*. The crude product was purified by flash chromatography (,ethyl acetate/petroleum ether; 5:2). The combined fractions were evaporated leading to the pure product as a light yellow powder.

Yield: 60%

M.W.: 432.58; $C_{21}H_{20}ON_2ClBr$

M.P.:145-147°C

^{1}H NMR (200 MHz, $CDCl_3$): δ 7.74 (s, 1H, Ar), 7.35-7.06 (m, 6, Ar, CH=C), 6.46-6.45 (d, 1H, C=CH), 4.92-4.86 (m, 1H), 4.42-4.31 (m, 1H, CH-N), 4.07-4.00 (m, 1H), 3.76 (s, 2H), 3.26-3.13 (m, 2H), 2.82-2.69 (m, 2h), 2.16-1.89 (m, 2H,).

tert-Butyl 4-(5-cyano-1H-indol-1-yl)piperidine-1-carboxylate (24)

Tert-butyl 4-(5-bromo-1*H*-indol-1-yl)piperidine-1-carboxylate **(21)** (0.57 g, 1.5 mmol), potassium ferrocyanide trihydrate (0.253 g, 0.6 mmol) and tetrakis(triphenylphosphyne)palladium(0) (0.05 g, 0.375 mmol) were charged in a vial which was capped, evacuated and filled with nitrogen. Then, 4.5 mL of a solution of water/*tert*-butanol (1:1) and 56 µL (0.375 mmol, d=1.018 g/mL) of DBU were added. The solution obtained was stirred at room temperature for 10 min and subsequently it was heated at 85°C in a pre-heated bath oil for 24 h. The reaction was filtered and the cake was rinsed with 20 mL of methanol and 20 mL of dichloromethane. The solution obtained was dried over magnesium sulfate, filtrated and evaporated *in vacuum*. The crude mixture was adsorbed on silica gel and purified by flash chromatography (ethyl acetate/petroleum ether 1:4). The combined fractions were evaporated leading to the pure product as a white powder

Yield: 80%

M.W.: 326.33; $C_{18}H_{23}O_2N_3$

M.P.: 121-123 °C

^{1}H NMR (200 MHz, $CDCl_3$): δ 7.98 (s, 1H, Ar), 7.43-7.42 (d, 2H), 7.31-7.29 (d, 1H), 6.62-6.60 (d, 1H), 4.44-4.43 (m, 1H), 2.98-2.86 (m, 3H), 2.10-1.99 (m, 6H), 1.41 (s, 9H).

^{13}C NMR (200 MHz, DMSO-d_6): 153.07 (C=O), 136.16 (CH), 127.25 (CH_2), 127.02 (CH_2), 125.38 (CH_2), 122.98 (CH_2), 119.98 (C), 110.52 (CH), 101.69 (CH_2), 100.58 (CH), 78.24 (CH_2), 51.86 (CH_2), 31.26 (CH_3).

4-(5-cyano-1H-indol-1-yl)piperidine (25)

Tert-butyl 4-(5-cyano-1H-indol-1-yl)piperidine-1-carboxylate **(24)** (0.33 g, 1 mmol) was dissolved in 5 mL of a methanol/ethyl acetate solution (3:1) and then 1 mL of hydrochloric acid 32% was added. The solution was stirred at 30 °C for 3 h. Then the reaction was quenched with a saturated solution of sodium bicarbonate (15 mL) until pH=8 leading to a precipitate. After filtration and drying over overnight, the titled compound was collected as a white powder

Yield: 90 %

M.W.:225.03; $C_{14}H_{14}N_3$

M.P.: 148-150°C

^{1}H NMR (200 MHz, DMSO-d_6): δ 8.09 (s, 1H, Ar), 7.82-7.47 (m, 4H), 6.64 (s, 1H), 4.71 (m 2H), 3.32-3.26 (m, 3H), 3.10-2.96 (m, 3H).

1-{1-[(*p*-chlorophenyl)acetyl]piperidin-4-yl}-1*H*-indole-5-carbonitrile (26a)

0.225 g (1.0 mmol) of 4-(5-cyano-1H-indol-1-yl)piperidine **(25)** were dissolved in 1 mL of DMF and 7 mL of THF. The solution obtained was cooled at 0 °C and added of 600 µL (4.3 mmol, d=0.726 g/mL) of triethylamine and 179 µL (1.2 mmol, d=1.292 g/mL) of *p*-chlorophenylacetyl chloride. The reaction was stirred at 0 °C for 1 h and kept to room temperature overnight. Then cold water was added and the crude product was extracted with chloroform which was dried over sulfate magnesium and filtered. The crude product was purified by flash chromatography (ethyl acetate). The combined fractions were evaporated leading to the pure product as a white powder.

Yiled: 65%

M.W.: 377.56; $C_{22}H_{20}ON_3Cl$

M.P.:174-172°C

^{1}H NMR (200 MHz, $CDCl_3$): δ 8.07-8.06 (d, 1H, Ar), 7.78-7.73 (d, 1H), 7.67-7.66 (d, 1H, Ar), 7.49-7.23 (m, 7H), 6.61-6.60 (d, 1H, C=CH), 4.76-4.75 (m, 2H), 3.31 (s, 2H), 3.31-3.22 (m, 3H), 1.96-1.89 (m, 2H).

2-(*p*-chlorophenyl)-1-{4-[5-(1*H*-tetrazol-5-yl)-1*H*-indole -1-yl]piperidin-1-yl}ethanone (27a)

A screw cap vial was charged with 0.094 g (0.25 mmol) of 1-{1-[(p-chlorophenyl)acetyl]piperidin-4-yl}-1*H*-indole-5-carbonitrile **(26a)**, 70 µL (0.5 mmol, d=0.868 g/ml) of azido(trimethyl)silane and 125 µL (0.125 mmol) of a 1M solution of TBAF in THF, under nitrogen. The mixture was stirred at 120 °C for 48 h. Then the crude mixture (brown semisolid) was cooled at room temperature and washed with a 2M aqueous solution of hydrochloric acid (3 X 5 mL) leading a green precipitate. The solid was filtrated and washed with water and purified by flash chromatography (ethyl acetate). The combined fractions were evaporated leading to the pure product as a white powder.

Yield: 16 %

M.W.: 424.9; $C_{22}H_{21}ON_6Cl$

M.P.: 214-216°C

^{1}H NMR (200 MHz, DMSO-d_6): δ 8.24(s, 1H, Ar), 7.78 (m, 2H,), 7.35(s, 1H, Ar), 7.29-7.25 (m, 4H), 6.619 (s, 1H, CH=C), 4.61 (m, 1H), 3.77-3.30 (m, 2H), 2.47 (m, 2H), 1.92-1.48 (m, 6H).

^{13}C NMR (200 MHz, DMSO-d_6): δ 173.85 (C=O), 141.89 (C), 140.46 (CH_2), 133.54 (CH_2), 132.24 (C), 125.25 (CH), 120.76 (C), 116.21 (CH), 107.63 (CH), 73.14 (CH_2), 73.13 (CH_2), 58.09 (CH), 50.22 (CH), 37.82 (CH).

tert-Butyl 4-(5-bromo-2,3-dioxo-2,3-dihydro-1*H*-indol-1-yl)piperidine-1-carboxylate (28)

An amount of 0.5 g (1.31 mmol) of tert-butyl 4-(5-bromo-1*H*-indol-1-yl)piperidine-1-carboxylate **(21)** was solubilized in 6 mL of acetone, 13 mL of acetic acid and 4.5 mL of water. The solution was slowly added of (over 45 min) 1.7 g (13 mmol) of chromium(VI) oxide. The reaction mixture was stirred at room temperature for 2 h, and added of ice and extracted with dichloromethane. The organic phases were washed with water and saturated solution of sodium bicarbonate and dried over magnesium sulfate. The solvent was removed *in vacuum* and the residue was purified by flash chromatography (*n*-hexane/ethyl acetate; 3:1). The combined fractions were evaporated leading to the pure product as an orange powder.

Yield: 28 %

M.W.: 409.32; $C_{18}H_{19}O_2N_2Br$

M.P.:165-167°C

^{1}H NMR (200 Mhz, $CDCl_3$): δ 7.41-7.34 (m, 2H, Ar), 7.04-6.99 (d, 1H, Ar), 4.19 (m, 1H), 3.62-3.30 (m, 2H), 3.21-3.05 (m, 4H), 2.67-2.55 (m, 2H), 1.23 (s, 9H).

tert-Butyl 4-(5-cyano-2,3-dioxo-2,3-dihydro-1*H*-indol-1-yl)piperidine-1-carboxylate (29)

tert-Butyl 4-(5-bromo-2,3-dioxo-2,3-dihydro-1*H*-indol-1-yl)piperidine-1-carboxylate **(28)** (0.17 g, 0.42 mmol), potassium ferrocyanide trihydrate (0.71 g, 0.17 mmol) and tetrakis(triphenylphosphyne)palladium(0) (0.02 g, 0.01 mmol) were charged in a vial, capped, evacuated and filled with nitrogen. 2 mL of a solution of water/*tert*-butanol (1:1) and 16 µL (0.1 mmol, d=1.018 g/mL) of DBU were added and stirred at room temperature for 10 min. Then the mixture was heated at 85°C in a pre-heated bath oil and stirred for 24 h. The reaction mixture was filtered and the cake was rinsed with 20 mL of methanol and 20 mL of dichloromethane. The solution obtained was dried over magnesium sulfate, filtrated and solvents removed in vacuum. The crude product was brown oil hardly to purify.

REFERENCES

1. Hanada K.; Serine palmitoyltransferase, a key enzyme of sphingolipid metabolism; *Biochim Biophys Acta*.; 2003 Jun 10; 1632(1-3); 16-30.
2. Yard BA, Carter LG, Johnson KA *et al.; J Mol Biol*.; 2007 Jul 27; 370(5); 870-86.
3. Hannun YA, Luberto; C. Ceramide in the eukaryotic stress response; *Trends Cell Biol*.; 2000 Feb; 10(2); 73-80.
4. Mathias S, Peña LA, Kolesnick; RN Signal transduction of stress via ceramide; *Biochem J*.; 1998 Nov 1; 335 (Pt 3); 465-80.
5. Spiegel S, Merrill AH Jr; Sphingolipid metabolism and cell growth regulation; *FASEB J*.; 1996 Oct; 10(12); 1388-97.
6. London E, Brown DA; Insolubility of lipids in triton X-100: physical origin and relationship to sphingolipid/cholesterol membrane domains (rafts); *Biochim Biophys Acta*.; 2000 Nov 23; 1508(1-2); 182-95.
7. Hanada K, Nishijima M, Akamatsu Y; Both sphingolipids and cholesterol participate in the detergent insolubility of alkaline phosphatase, a glycosylphosphatidylinositol-anchored protein, in mammalian membranes; *J Biol Chem*.; 1995 Mar 17; 270(11); 6254-60.
8. Fukasawa M, Nishijima M, Itabe H, *et al;* Reduction of sphingomyelin level without accumulation of ceramide in Chinese hamster ovary cells affects detergent-resistant membrane domains and enhances cellular cholesterol efflux to methyl-beta – cyclodextrin; *J Biol Chem*. ; 2000 Nov 3; 275(44); 34028-34.
9. Helms JB, Zurzolo C.; Lipids as targeting signals: lipid rafts and intracellular trafficking; *Traffic.;* 2004 Apr; 5(4):247-54.
10. Norlén L.; Skin barrier structure and function: the single gel phase model; *J Invest Dermatol*.; 2001 Oct; 117(4); 830-6.
11. Alfred H. Merrill, Jr.; Sphingolipid and Glycosphingolipid Metabolic Pathways in the Era of Sphingolipidomics; *Chem Rev*.; 2011 October 12; 111(10); 6387–6422.
12. Jonathan Lowther, James H. Naismith, Teresa M. Dunn *et al.;* Structural, mechanistic and regulatory studies of serine palmitoyltransferase; *Biochemical Society Transactions*; (2012) 40; (547–554).
13. Braun PE, Snell EE.; Keto intermediates in synthesis of sphingosine and dihydrosphingosine by cell-free extracts of Hansenula ciferri; *J Biol Chem*.; *1968* Jul 25; *243*(14); *3775–3783*;
14. Stoffel W, LeKim D, Sticht G; Biosynthesis of dihydrosphingosine in vitro; *Physiol Chem.;* 1968 May; 349(5); 664-70.

15. J .N. Kanfe; Sphingolipid metabolism: J.N. Kanfer, S. Hakomori (Eds.), *Sphingolipid Biochemistry, Plenum*, New York, NY, USA; 1983; pp. 167–247.
16. Dickson RC.; Sphingolipid functions in *Saccharomyces cerevisiae*: comparison to mammals; *Annu. Rev. Biochem.*; 1998; 67; 27-48.
17. Zabini, Mead JF.; The biosynthesis of sphingosine I. The utilization of carboxyl-labeled acetate; *J Biol Chem.* ; 1953 Nov; 205(1); 271-7.
18. Ikushiro H, Hayashi H, Kagamiyama H.; A water-soluble homodimeric serine palmitoyltransferase from *Sphingomonas paucimobilis* EY2395T strain. Purification, characterization, cloning, and overproduction; *J Biol Chem.*; 2001 May 25; 276(21); 18249-56.
19. Yard BA, Carter LG, Johnson KA *et al.*; The structure of serine palmitoyltransferase: gateway to sphingolipid biosynthesis; *J. Mol. Biol.*; 2007 Jul 27; 370(5); 870-86.
20. Ikushiro H, Islam MM, Okamoto A.; Structural insights into the enzymatic mechanism of serine palmitoyltransferase from *Sphingobacterium multivorum; J Biochem.*; 2009 Oct; 146(4); 549-62.
21. Geiger O, González-Silva N, López-Lara *et al.;* Amino acid-containing membrane lipids in bacteria*; Prog. Lipid Res.;* 2010 Jan; 49(1); 46-60.
22. Lowther J, Naismith JH, Dunn TM *et al.*; Structural, mechanistic and regulatory studies of serine palmitoyltransferase; *Biochem Soc Trans.*; 2012 Jun 1; 40(3); 547-54.
23. Weiss B, Stoffel W.; Human and murine serine-palmitoyl-CoA transferase--cloning, expression and characterization of the key enzyme in sphingolipid synthesis; *Eur. J. Biochem.*; 1997 Oct 1; 249(1); 239-47.
24. Hanada K, Hara T, Nishijima M, *et al.;* A mammalian homolog of the yeast LCB1 encodes a component of serine palmitoyltransferase, the enzyme catalyzing the first step in sphingolipid synthesis; *J. Biol. Chem.*; 1997 Dec 19; 272(51); 32108-14.
25. Hanada K, Hara T, Fukasawa M *et al.;* Mammalian cell mutants resistant to a sphingomyelin-directed cytolysin. Genetic and biochemical evidence for complex formation of the LCB1 protein with the LCB2 protein for serine palmitoyltransferase; *J. Biol. Chem.*; 1998 Dec 11; 273(50); 33787-94.
26. Mandon EC, Ehses I, Rother J, *et al.;* Subcellular localization and membrane topology of serine palmitoyltransferase, 3-dehydrosphinganine reductase, and

sphinganine N-acyltransferase in mouse liver; *J Biol Chem.*; 1992 Jun 5; 267(16); 11144-8.

27. Han G, Gupta SD, Gable K, Niranjanakumari S *et al.;* Identification of small subunits of mammalian serine palmitoyltransferase that confer distinct acyl-CoA substrate specificities; *Proc. Natl. Acad. Sc*i. U S A.; 2009 May 19; 106(20); 8186-91.
28. Breslow DK, Collins SR, Bodenmiller B *et al.;* Orm family proteins mediate sphingolipid homeostasis; *Nature*; 2010 Feb 25; 463(7284); 1048-53.
29. Hanada K, Hara T, Nishijima M.; Purification of the serine palmitoyltransferase complex responsible for sphingoid base synthesis by using affinity peptide chromatography techniques; *J Biol Chem.*; 2000 Mar 24; 275(12); 8409-15.
30. K. Hanada, T. Hara, M. Nishijima; Purification of the serine palmitoyltransferase complex responsible for sphingoid base synthesis by using affinity peptide chromatography techniques; *J. Biol. Chem.*; 2000; 275; 8409– 8415.
31. Zweerink MM, Edison AM, Wells GB, *et al;* Characterization of a novel, potent, and specific inhibitor of serine palmitoyltransferase*; J Biol Chem.*; 1992 Dec 15; 267(35); 25032-8;
32. Shuh Kobayashi, Takayuki Furuka, Takaomi Hayashi *et al. ;* Catalytic Asymmetric Syntheses of Antifungal Sphingofungins and Their Biological Activity as Potent Inhibitors of Serine Palmitoyltransferase (SPT); *J.Am.Chem.Soc; 1998; 120; 908-919.*
33. Miyake Y, Kozutsumi Y, Nakamura S *et al.;* Serine palmitoyltransferase is the primary target of a sphingosine-like immunosuppressant, ISP-1/myriocin; *Biochem. Biophys. Res. Commun.*; 1995 Jun 15;211(2); 396-403;
34. Arun K. Ghosh and Jorden Kass.; A Stereoselective Synthesis of (−)-Viridiofungin A Utilizing a TiCl4-Promoted Asymmetric Multicomponent Reaction; *J. Antibiotics.* 1997; 50; 339–343;
35. Jonathan Lowther, Ashley E. Beattie, Pat R. R. Langridge-Smith *et al.;* L-Penicillamine is a mechanism-based inhibitor of serine palmitoyltransferase by forming a pyridoxal-50-phosphate-thiazolidine adduct; *Med. Chem. Commun.*; 2012; 3; 1003.
36. K S Sundaram and M Lev; Comparative inhibition of bacterial and microsomal 3-ketodihydrosphingosine synthetases by L-cycloserine and other inhibitors; *Antimicrob Agents Chemother.;* 1984 August; 26(2): 211–213.

37. Kimberly A.Medlock and Alfred H.Merrill,Jr; Inhibition of serine palmitoyltransferase and long-chain base biosynthesis in intact Chinese hamster ovary cells by β-chloroalanine; *Biochemistery;* 27 (1988); 7079-7084.
38. Fenn TD, Stamper GF, Morollo AA *et al.*; Different modes of action of inhibitors of bacterial D-amino acid transaminase. A target enzyme for the design of new antibacterial agents; *J Biol Chem;*. 1981 May 10; 256(9); 4263-8.
39. Ringe D.; A side reaction of alanine racemase: transamination of cycloserine; *Biochemistry*.; 2003 May 20;42(19); 5775-83.
40. Malashkevich VN, Strop P, Keller JW *et al.;* Crystal structures of dialkylglycine decarboxylase inhibitor complexes; *J Mol Biol.*; 1999 Nov 19; 294(1); 193-200.
41. Neuhaus FC, Lynch Jl.; The enzymatic synthesis of d-alanyl-d-alanine. 3. On the inhibition of d-alanyl-d-alanine synthetase by the antibiotic d-cycloserine; *Biochemistry*.; 1964 Apr; 3; 471-80.
42. A Sheinin, S Shavit, M Benveniste; Subunit specificity and mechanism of action of NMDA partial agonist d-cycloserine; *Neuropharmacology;* 2001; 41; 151-158.
43. Sundaram KS, Lev M.; Comparative inhibition of bacterial and microsomal 3-ketodihydrosphingosine synthetases by L-cycloserine and other inhibitors; *Antimicrob Agents Chemother.;* 1984 Aug; 26(2); 211-3.
44. Ikushiro H, Hayashi H, Kagamiyama H; Reactions of serine palmitoyltransferase with serine and molecular mechanisms of the actions of serine derivatives as inhibitors; *Biochemistry;* 2004, 43(4):1082-1092.
45. Lowther J, Yard BA, Johnson KA, Carter LG *et al.*; Inhibition of the PLP-dependent enzyme serine palmitoyltransferase by cycloserine: evidence for a novel decarboxylative mechanism of inactivation; *Mol Biosyst.*; 2010 Sep; 6(9); 1682-93.
46. Wadsworth JM, Clarke DJ, McMahon SA, Lowther JP *et al.;* The Chemical Basis of Serine Palmitoyltransferase Inhibition by Myriocin; *J Am Chem Soc*.; 2013 Sep 11.
47. Strettoi E, Gargini C, Novelli E, *et al.;* Inhibition of ceramide biosynthesis preserves photoreceptor structure and function in a mouse model of retinitis pigmentosa; *Proc Natl Acad Sci U S A. 2010 Oct* 26;107(43):18706-11.
48. Hartong DT, Berson EL, Dryja TP; Retinitis pigmentosa; *Lancet*. 2006 Nov 18; 368(9549); 1795-809.
49. Corrochano S, Barhoum R, Boya P. *et al.;* Attenuation of vision loss and delay in apoptosis of photoreceptors induced by proinsulin in a mouse model of retinitis pigmentosa; *Invest Ophthalmol Vis Sci.*; 2008 Sep; 49(9); 4188-94.

50. Tuson M, Marfany G, Gonzàlez-Duarte R.; Mutation of CERKL, a novel human ceramide kinase gene, causes autosomal recessive retinitis pigmentosa (RP26); *Am J Hum Genet.;* 2004 Jan; 74(1); 128-38.
51. Acharya U, Patel S, Koundakjian E, *et al.;* Modulating sphingolipid biosynthetic pathway rescues photoreceptor degeneration; *Science.*; 2003 Mar 14;299(5613); 1740-3.
52. Sanvicens N, Cotter TG.; Ceramide is the key mediator of oxidative stress-induced apoptosis in retinal photoreceptor cells; *J Neurochem.*; 2006 Sep; 98(5); 1432-44.
53. Chang B, Hawes NL, Pardue MT *et al.;* Two mouse retinal degenerations caused by missense mutations in the beta-subunit of rod cGMP phosphodiesterase gene*; Vision Res.*; 2007 Mar; 47(5); 624-33
54. Barhoum R, Martínez-Navarrete G, Corrochano S, Germain F *et al.;* Functional and structural modifications during retinal degeneration in the rd10 mouse; *Neuroscience.;* 2008 Aug 26;155(3); 698-713.
55. Vassar, R., Bennett, B.D., Babu-Kahn, S., *et al.* ?-Secretase cleavage of Alzheimer's amyloid precursor protein by the transmembrane aspartic protease BACE. *Science;* **1999;** *286*:735-741.
56. Arnold, S.E., Hyman, B.T., Flory, J., Damasio, A.R *et al.;* The topographical and neuroanatomical distribution of neurofibrillary tangles and neuritic plaques in the cerebral cortex of patients with Alzheimer's disease. *Cereb. Cortex*, **1991,** *1*:103-116
57. Braak, H., and Braak, E.; Pathology of Alzheimer's disease; *Neurodegenerative Diseases.*; Saunders, Philadelphia; **1994;** pp. 585-614
58. Burger's medicinal chemistery, 6th edition
59. Goodman&Gilman, farmacological bases of therapy, 11th edition
60. Furuya S, Mitoma J, Makino A, *et al.;* Ceramide and its interconvertible metabolite sphingosine function as indispensable lipid factors involved in survival and dendritic differentiation of cerebellar Purkinje cells; *J Neurochem.*; 1998 Jul;71(1); 366-77.
61. Irie F, Hirabayashi Y.; Application of exogenous ceramide to cultured rat spinal motoneurons promotes survival or death by regulation of apoptosis depending on its concentrations*; J Neurosci Res.;* 1998 Nov 15; 54(4); 475-85.
62. Brugg B, Michel PP, Agid Y, *et al.;* Ceramide induces apoptosis in cultured mesencephalic neurons; J *Neurochem.*; 1996 Feb;66(2):733-9.

63. Mangoura D, Dawson G.; Programmed cell death in cortical chick embryo astrocytes is associated with activation of protein kinase PK60 and ceramide formation*; J Neurochem*.; 1998 Jan; 70(1; 130-8.
64. Sastry PS, Rao KS ; Apoptosis and the nervous system; *J Neurochem*. 2000 Jan; 74(1); 1-20.
65. Satoi H, Tomimoto H, Ohtani R, *et al.;* Astroglial expression of ceramide in Alzheimer's disease brains: a role during neuronal apoptosis; *Neuroscience*.; 2005; 130(3); 657-66.
66. Gulbins E, Kolesnick R.; Raft ceramide in molecular medicine; *Oncogene*; 2003 Oct 13; 22(45); 7070-7.
67. Kalvodova L, Kahya N, Schwille P *et al.*; Lipids as modulators of proteolytic activity of BACE: involvement of cholesterol, glycosphingolipids, and anionic phospholipids in vitro; *J Biol Chem*.; 2005 Nov 4;280(44); 36815-23.
68. Sun X, Beglopoulos V, Mattson MP, *et al.;* Hippocampal spatial memory impairments caused by the familial Alzheimer's disease-linked presenilin 1 M146V mutation; *Neurodegener Dis*. ; 2005;2(1):6-15.
69. Puglielli L, Ellis BC, Saunders AJ; Ceramide stabilizes beta-site amyloid precursor protein-cleaving enzyme 1 and promotes amyloid beta-peptide biogenesis; *J Biol Chem*.; 2003 May 30; 278(22); 19777-83.
70. Julien C, Tremblay C, Phivilay A, *et al.;* High-fat diet aggravates amyloid-beta and tau pathologies in the 3xTg-AD mouse model; *Neurobiol Aging*.; 2010 Sep; 31(9); 1516-31.
71. Lovell MA, Ehmann WD, Mattson MP *et al.;* Elevated 4-hydroxynonenal in ventricular fluid in Alzheimer's disease; *Neurobiol Aging;* 1997 Sep-Oct; 18(5); 457-61.
72. Papaioannou N, Tooten PC, van Ederen AM, *et al.;* Immunohistochemical investigation of the brain of aged dogs. I. Detection of neurofibrillary tangles and of 4-hydroxynonenal protein, an oxidative damage product, in senile plaques; *Amyloid.*; 2001 Mar; **8**(1); **11-21**.
73. Mattson MP.; Modification of ion homeostasis by lipid peroxidation: roles in neuronal degeneration and adaptive plasticity; *Trends Neurosci.*; 1998 Feb; 21(2); 53-7.

74. Roy G. Cutler, Jeremiah Kelly, Kristin Storie, *et al.;* Involvement of oxidative stress-induced abnormalities in ceramide and cholesterol metabolism in brain aging and Alzheimer's diseas; *PNAS* ; February 17, 2004; vol. 101; no. 7; 2070–2075
75. **Haughey** NJ, Bandaru VV, Bae M, *et al.;* Roles for dysfunctional sphingolipid metabolism in Alzheimer's disease neuropathogenesis; *Biochim Biophys Acta.;* 2010 Aug; 1801(8); 878-86.
76. Hur JY, Welander H, Behbahani H, *et al.;* Active gamma-secretase is localized to detergent-resistant membranes in human brain; *FEBS J;* 2008 Mar;275(6):1174-87.
77. Shen Y, Sullivan T, **Lee** CM, Meri S. *et al.;* Induced expression of neuronal membrane attack complex and cell death by Alzheimer's beta-amyloid peptide; *Brain Res.;* 1998 Jun 15;796(1-2); 187-97.
78. Vetrivel KS, Cheng H, Lin W, *et al.;* Association of gamma-secretase with lipid rafts in post-Golgi and endosome membranes; *J Biol Chem.;* 2004 Oct 22;279(43):44945-54.
79. Vetrivel KS, Cheng H, Kim SH *et al.;* Spatial segregation of gamma-secretase and substrates in distinct membrane domains; *J Biol Chem.*; 2005; Jul 8; 280(27):25892-900.
80. Hirosha Geekiyanage, Aditi Upadhye, Christina Chan; Inhibition of serine palmitoyltransferase reduces Ab and tau hyperphosphorylation in a murine model: a safe therapeutic strategy for Alzheimer's disease; *Neurobiology of Aging xxx*; (2013) 1e15.
81. Sundaram KS, Lev M.; The long-term administration of L-cycloserine to mice: specific reduction of cerebroside level; *Neurochem Res;* 1989 Mar; 14(3); 245-8.
82. Tsai GE, Falk WE, Gunther J *et al.;* Improved cognition in Alzheimer's disease with short-term D-cycloserine treatment.; *Am J Psychiatry*; 1999 Mar; 156(3); 467-9.
83. ; Janus C, Phinney AL, Chishti MA *et al.;* New developments in animal models of Alzheimer's disease; *Curr Neurol Neurosci Rep.*; 2001 Sep; 1(5); 451-7.
84. Auer-Grumbach M.; Hereditary sensory neuropathy type I; *Orphanet J Rare Dis*. 2008 Mar 18; 3; 7.
85. Dawkins JL, Hulme DJ, Brahmbhatt SB *et al.;* Mutations in SPTLC1, encoding serine palmitoyltransferase, long chain base subunit-1, cause hereditary sensory neuropathy type I; *Nat Genet;*. 2001 Mar; 27(3); 309-12.
86. ; Bejaoui K, Wu C, Scheffler MD *et al.;* SPTLC1 is mutated in hereditary sensory neuropathy, type 1; *Nat Genet*.; 2001 Mar; 27(3); 261-2.

87. Bi H, Gao Y, Yao S, Dong M *et al.;* Hereditary sensory and autonomic neuropathy type I in a Chinese family: British C133W mutation exists in the Chinese; *Neuropathology*; 2007 Oct;27(5); 429-33.
88. Klein CJ, Wu Y, Kruckeberg KE *et al.;* SPTLC1 and RAB7 mutation analysis in dominantly inherited and idiopathic sensory neuropathies; *J Neurol Neurosurg Psychiatry*; 2005 Jul; 76(7); 1022-4.
89. Houlden H, King R, Blake J; Pathological and genetic characterization of hereditary sensory and autonomic neuropathy type 1 (HSAN I); *Brain*; 2006 Feb;129(Pt 2); 411-25..
90. Hornemann T, Penno A, Richard S *et al.;* A systematic comparison of all mutations in hereditary sensory neuropathy type I (HSAN I) reveals that the G387A mutation is not disease associated;, *Neurogenetics*; 2009 Apr;10(2):135-43.
91. Hojjati MR, Li Z, Jiang XC.; Serine palmitoyl-CoA transferase (SPT) deficiency and sphingolipid levels in mice; *Biochim Biophys Acta;* 2005 Oct 15; 1737(1); 44-51.
92. Tani M, Ito M, Igarashi Y.; Ceramide/sphingosine/sphingosine 1-phosphate metabolism on the cell surface and in the extracellular space; *Cell Signal;* 2007 Feb;19(2):229-37.
93. Penno A, Reilly MM, Houlden H *et al.;* Hereditary sensory neuropathy type 1 is caused by the accumulation of two neurotoxic sphingolipids; *J Biol Chem*.; 2010 Apr 9; 285(15); 11178-87.
94. Lee YS, Choi KM, Choi MH; Serine palmitoyltransferase inhibitor myriocin induces growth inhibition of B16F10 melanoma cells through G(2) /M phase arrest; *Cell Prolif*.; 2011 Aug; 44(4); 320-9.
95. Helmbach H, Rossmann E, Kern MA; Drug-resistance in human melanoma; *Int J Cancer*; 2001 Sep 1; 93(5); 617-22.
96. Soengas MS, Capodieci P, Polsky D *et al.;*Inactivation of the apoptosis effector Apaf-1 in malignant melanoma; *Nature*; 2001 Jan 11; 409(6817); 207-11;
97. Modrak DE, Gold DV, Goldenberg DM ; Sphingolipid targets in cancer therapy; *Mol Cancer Ther*.; 2006 Feb; 5(2); 200-8.;
98. Kok JW, Sietsma H.; Sphingolipid metabolism enzymes as targets for anticancer therapy; *Curr Drug Targets*; 2004 May; 5(4); 375-82.

99. Olivera A, Spiegel S.; Sphingosine-1-phosphate as second messenger in cell proliferation induced by PDGF and FCS mitogens; *Nature*; 1993 Oct 7; 365(6446); 557-60.

100. Sekine Y, Suzuki K, Remaley AT.; HDL and sphingosine-1-phosphate activate stat3 in prostate cancer DU145 cells via ERK1/2 and S1P receptors, and promote cell migration and invasion; *Prostate*; 2011 May 15; 71(7); 690-9.

101. Hojjati MR, Li Z, Zhou H *et al.;* Effect of myriocin on plasma sphingolipid metabolism and atherosclerosis in apoE-deficient mice; *J Biol Chem*.; 2005 Mar 18;280(11); 10284-9.

102. Glaros EN, Kim WS, Wu BJ *et al.;* Inhibition of atherosclerosis by the serine palmitoyl transferase inhibitor myriocin is associated with reduced plasma glycosphingolipid concentration; *Biochem Pharmacol*.; 2007 May 1;73(9); 1340-6.

103. Miyake Y, Kozutsumi Y, Nakamura S. *et al.;*Serine palmitoyltransferase is the primary target of a sphingosine-like immunosuppressant, ISP-1/myriocin; *Biochem. Biophys. Res. Commun*.; 1995 Jun 15; 211(2); 396-403.

104. Hainaut P, Hollstein M; p53 and human cancer: the first ten thousand mutations*; Adv Cancer Res.* 2000; 77; 81-137.

105. Schwartz GK.; Development of cell cycle active drugs for the treatment of gastrointestinal cancers: a new approach to cancer therapy; *J Clin Oncol*.; 2005 Jul 10; 23(20); 4499-508.

106. Matsuoka S, Huang M, Elledge SJ; Linkage of ATM to cell cycle regulation by the Chk2 protein kinase; Science; 1998 Dec 4;282(5395); 1893-7.

107. Strausfeld U, Labbé JC, Fesquet D *et al.;* Dephosphorylation and activation of a p34cdc2/cyclin B complex in vitro by human CDC25 protein; *Nature*; 1991 May 16; 351(6323); 242-5.

108. Lee YS, Choi KM, Choi MH *et al.;* Serine palmitoyltransferase inhibitor myriocin induces growth inhibition of B16F10 melanoma cells through G(2) /M phase arrest; *Cell Prolif*.; 2011 Aug;44(4):320-9.

109. Meier F, Schittek B, Busch S, *et al.;* The RAS/RAF/MEK/ERK and PI3K/AKT signaling pathways present molecular targets for the effective treatment of advanced melanoma; *Front Biosci*. 2005 Sep 1; 10; 2986-3001.

110. Lee YS, Choi KM, Choi MH *et al.;* Serine palmitoyltransferase inhibitor myriocin induces growth inhibition of B16F10 melanoma cells through G(2) /M phase arrest; *Cell Prolif.;* 2011 Aug; 44(4); 320-9.

111. *Gary Louis Bolton, 17 lug 2008; Inhibitors of serine palmitoyltransferase (WO 2008084300 A1).*

112. David Amantini, Romina Beleggia, Francesco Fringuelli *et al.; TBAF-Catalyzed Synthesis of 5-Substituted 1H-Tetrazoles under Solventless Conditions;* Volume 69; Issue 8; pp 2896–2898.

113. Srinivas Rao Vankadari, Devender Mandala,Jalapathi Pochampalli *et al.*; Synthesis, evaluation of antimicrobial activity, and molecular modeling of novel 2-((4-(2H-benzo[d] [1,2,3] triazol-2-yl)piperidin-1-yl)methyl)-5-substituted phenyl-1,3,4-oxadiazoles; Medicinal Chemistry Research© Springer Science+Business Media New York 201310.1007/s00044-013-0573-9.

114. M. Sassatelli, F. Bouchikhi, S. Messaoudi *et al. ; Synthesis and antiproliferative activities of diversely substituted glycosyl-isoindigo derivatives; European Journal of Medicinal Chemistery; 41 (2006); 88-100.*

115. Journal of organic chemistery;11; 1987;605.

116. Khan MN.; Suggested Improvement in the Ing-Manske Procedure and Gabriel Synthesis of Primary Amines: Kinetic Study on Alkaline Hydrolysis of N-Phthaloylglycine and Acid Hydrolysis of N-(o-Carboxybenzoyl)glycine in Aqueous Organic Solvents; J Org Chem. 1996 Nov 15;61(23):8063-8068.

117. Dengyou Zhang, Haifeng Sun, Lei Zhang *et al. An expedient Pd/DBU mediated cyanation of aryl/heteroaryl bromides with K4[Fe(CN)6]*; Chem. Commun.; 2012; **48**; 2909–2911.

118. Li X, Liu B, Xu X, Chmielewski PJ. *;DDQ-supported alkoxylation of 2-aza-21-carbaporphyrin and noncatalyzed transetherification of its 3,21-dialkoxy derivatives; J Org Chem. 2012 Sep 21;77(18):8206-19*